NATIONAL ADVISORY COMMITTEE FOR AERONAUTICS

TECHNICAL NOTE 2787

AIRFOIL PROFILES FOR MINIMUM PRESSURE DRAG AT SUPERSONIC VELOCITIES - APPLICATION OF SHOCK-EXPANSION THEORY, INCLUDING CONSIDERATION OF HYPERSONIC RANGE

By Dean R. Chapman

Ames Aeronautical Laboratory
Moffett Field, Calif.

Washington
September 17, 1952

iV

NATIONAL ADVISORY COMMITTEE FOR AERONAUTICS

TECHNICAL NOTE 2787

AIRFOIL PROFILES FOR MINIMUM PRESSURE DRAG AT SUPERSONIC VELOCITIES - APPLICATION OF SHOCK-EXPANSION THEORY, INCLUDING CONSIDERATION OF HYPERSONIC RANGE

By Dean R. Chapman

SUMMARY

A theoretical investigation is made of airfoil profiles at supersonic velocities to determine the shapes having minimum pressure drag at zero lift for various given auxiliary conditions. Shock-expansion theory is employed, thereby extending the applicability of the results through the hypersonic range. Curves are presented for Mach numbers of 1.5, 2, 3, 4, 6, 8, and ∞ which enable the shape and the drag of an optimum profile to be determined readily if the base pressure is known from experiments. Examples are presented of optimum profiles determined with the aid of experimental base pressure data. Variations in profile shape are investigated to provide information on the degree to which deviations in shape from the optimum can be made without resulting in a significant drag increase.

A comparison of optimum profiles determined by the shock-expansion method of this report with corresponding profiles determined by the linearized-theory method of a previous report shows only small differences in shape at Mach numbers up to infinity even though the linearized theory at high supersonic Mach numbers breaks down completely insofar as the drag of the profile is concerned. The experimentally observed dependence of base pressure on trailing-edge thickness is found to have a significant effect on the shape and drag of optimum profiles of small thickness ratio. Curves are presented which show that for thin airfoils the use of a trailing-edge thickness considerably greater than the theoretical optimum can result in an excessive drag penalty at moderate supersonic Mach numbers, though not at hypersonic Mach numbers.

INTRODUCTION

In 1933 Saenger observed that for the extreme case of flow at infinite Mach number an airfoil designed to have minimum pressure drag

would have its maximum thickness at the trailing edge. (See reference 1.) A related result can be inferred from the numerical calculations of Ivey (reference 2) which indicate that the drag of a 10-percent-thick-wedge airfoil at a Mach number of 8 is less than that of a double-wedge airfoil having the same thickness ratio. In both of these cases the desirability of employing a thick trailing edge in conjunction with a small surface slope may be attributed to the fact that at hypersonic Mach numbers the suction forces (forces due to pressures below ambient) are small compared to the positive pressure forces, even when the suction force corresponds to a vacuum. Recently, Smelt (reference 3) has discussed this latter characteristic of hypersonic flow and its possible application to the determination of efficient airfoil shapes for use at very high Mach numbers. The investigations of Saenger, Ivey, and Smelt, however, do not provide general quantitative information on the airfoil profile having minimum pressure drag in hypersonic flow because of two limitations of their analyses: Airfoils having a trailing-edge thickness less than the maximum airfoil thickness were not considered, and the airfoil structural characteristics were not considered (comparisons were made on the basis of a given airfoil thickness).

At low and moderate supersonic Mach numbers the suction forces on an airfoil can amount to several times the positive pressure forces, particularly if an excessively thick trailing edge is employed. As a result, the optimum trailing-edge thickness in this lower Mach number range depends to a great extent on the base pressure. By presuming that the base pressure is known from experiments, and that the airfoil profile must satisfy a given structural requirement (such as a given section modulus or a given section moment of inertia), a method of calculating the profile of minimum pressure drag at zero lift has been developed by the present writer in reference 4. Although the basic equations developed in reference 4 for calculating such profiles are applicable to higher-order theories, a detailed solution was given only for the case of linearized supersonic flow.

Because of the well-known shortcomings of linearized theory, it was thought worthwhile to conduct an investigation parallel to that of reference 4 in which the shape and drag of optimum airfoils are determined from shock-expansion theory instead of linearized theory. Shock-expansion theory appears adequate for this purpose, particularly in view of the recent investigation of Eggers and Syvertson (reference 5) which indicates that shock-expansion calculations accurately determine surface pressures on thin airfoils in inviscid flow at Mach numbers from just above that for bow-wave attachment to infinity. From the viewpoint of the engineer who always has to make design compromises, it was thought desirable in the present study also to determine how much the optimum-profile shape can be altered, especially near the trailing edge, and still not increase the drag excessively. The purposes of the present investigation, therefore, were (1) to develop a usable method for determining the shape and drag of optimum profiles in the Mach number range beyond that covered adequately by linearized theory (step-by-step details involved in applying

the method developed are given in an appendix), and (2) to determine curves showing the rate at which the total pressure drag increases as the profile shape deviates from the optimum.

NOMENCLATURE

c	airfoil chord
c_d	pressure drag coefficient
C	constant depending on γ
h	trailing-edge thickness
H	dimensionless trailing-edge thickness $\left(\frac{h}{t}\right)$
I	given value of auxiliary integral $\left\{\int_0^c \left[\frac{y^n}{(t/2)^\sigma}\right]\frac{dx}{c}\right\}$
$\bar{I}$	dimensionless value of I $\left[\frac{I}{(t/2)^{n-\sigma}}\right]$
j_n	normalizing factor for $\xi(Y)$, defined by equation (10)
l	length of surface of constant thickness
L	dimensionless length of surface of constant thickness $\left(\frac{l}{s}\right)$
M	Mach number
n	parameter appearing in definition of I
p	pressure
p_t	total pressure
P	pressure coefficient $\left(\frac{p - p_\infty}{\frac{1}{2}\rho_\infty V_\infty^2}\right)$
Re	Reynolds number
s	chordwise distance from leading edge to first downstream position of maximum thickness
t	maximum thickness of airfoil
V	velocity
x	chordwise distance from leading edge to point on airfoil surface

y ordinate of upper surface of airfoil

X dimensionless distance $\left(\frac{x}{s}\right)$

Y dimensionless distance $\left(\frac{y}{t/2}\right)$

γ ratio of specific heats (1.40 for air)

λ arbitrary constant

ρ mass density

δ local angle of inclination of airfoil surface with respect to chord line ($\tan^{-1}y'$)

$\xi(Y)$ characteristic function determining optimum-profile shape, defined by equation (9)

$\eta(Y)$ characteristic function defined by equation (12)

Subscripts

o airfoil surface at leading edge

1 airfoil surface at trailing edge

∞ free stream

b base, or trailing edge, of airfoil

ca circular-arc biconvex airfoil having sharp trailing edge

Superscripts

$'$ differentiation with respect to x

ANALYSIS

Solution for Arbitrary Structural Requirement

As in reference 4, it is assumed throughout this analysis that the optimum airfoil has a sharp leading edge, a fixed chord length, and is set at the zero-lift angle. It also is assumed that the flow is a

purely supersonic two-dimensional flow of an inviscid, nonconducting, perfect gas. Since the surface pressures on the top and bottom of an airfoil can be calculated independently in a supersonic flow, it follows that at zero lift the optimum profile will be symmetrical about the chord line. The mathematical problem formulated is to find the airfoil ordinate function $y(x)$ which minimizes the pressure drag,

$$c_d = \frac{2}{c}\int_0^c Py'\,dx - P_b\frac{h}{c} \tag{1}$$

for a given value of the auxiliary integral

$$I = \frac{1}{c}\int_0^c \frac{y^n}{(t/2)^\sigma}\,dx \tag{2}$$

By selecting various values of the parameters n and σ, a wide variety of structural requirements can be represented for both thin-skin and solid-section structures. Some of the different structural criteria represented by equation (2) are:

n	σ	Structural criteria
1	0	given torsional stiffness, or torsional strength, of thin-skin structure (given cross-section area)
2	0	given bending stiffness of thin-skin structure
3	0	given bending stiffness or given torsional stiffness of solid-section structure
2	1	given bending strength of thin-skin structure
3	1	given bending strength of solid-section structure

Basic equations.- The equations which the optimum-airfoil ordinate function $y(x)$ must satisfy can be obtained by considering an infinitesimal variation in profile shape $\delta y(x)$ that is arbitrary except for the requirement that $\delta I = 0$. By also requiring that $\delta c_d = 0$ the following three equations result (see reference 4):

$$\frac{d}{dx}\left(P + y'\frac{\partial P}{\partial y'}\right) + \lambda n y^{n-1} = 0 \tag{3}$$

$$P_b = P_1 + y_1'\left(\frac{\partial P}{\partial y'}\right)_1 \tag{4}$$

$$\frac{l}{c} = \frac{\sigma}{n}\bar{I} \quad \left(\bar{I} \equiv I/(t/2)^{n-\sigma}\right) \tag{5}$$

In the derivation of these equations it was assumed that $P = P(y', y_o', M_\infty)$, but no particular functional form was assumed. Equation (3) is the differential equation which the airfoil ordinate function $y(x)$ must satisfy along the curved surfaces, for example, OA and BC in figure 1. A first integral

of this differential equation, satisfying the condition $y' = 0$ at $y = t/2$, can be obtained by multiplying both sides by y' and integrating.

$$y'^2 \frac{\partial P}{\partial y'} = \lambda[(t/2)^n - y^n] \tag{3a}$$

Equations (3) and (3a) involving the arbitrary constant λ do not apply to the straight midsection (AB in fig. 1) along which the airfoil thickness is constant. Equation (4), termed an end condition, represents the relation which must be satisfied between the base pressure coefficient P_b, the surface pressure coefficient P_1 just upstream of the trailing edge, and the corresponding surface slope y_1'. As will be seen this equation determines the optimum trailing-edge thickness. Equation (5) relates the optimum length of straight midsection l to the dimensionless value of the structural integral $\overline{I}$. This latter equation shows that the length of straight midsection is always zero when the auxiliary condition represents a given stiffness ($\sigma = 0$), but for the values of n considered is a sizable fraction of the chord when the auxiliary condition represents a given strength ($\sigma = 1$).

Solution for Y, H, and X.- From equation (3a) the constant λ is readily evaluated in terms of y_o'. There results

$$\lambda(t/2)^n = y_o'^2\left(\frac{\partial P}{\partial y'}\right)_o \tag{3b}$$

By employing the dimensionless variables $Y = y/(t/2)$ and $H = h/t$, equations (3a) and (3b) yield

$$Y^n = 1 - \frac{y'^2(\partial P/\partial y')}{y_o'^2(\partial P/\partial y')_o} \tag{6}$$

and hence

$$H^n = 1 - \frac{y_1'^2(\partial P/\partial y')_1}{y_o'^2(\partial P/\partial y')_o} \tag{7}$$

It is to be noted that the structure of these equations, and all subsequent ones, is such that the quantities P_b, I, and M_∞ which are presumed to be given do not appear as independent variables. Instead, they are related parametrically to the shape and drag of the optimum profile through the parameter y'. For example, equation (7) gives $H(y_1', y_o', M_\infty)$, and equation 4 gives $P_b(y_1', y_o', M_\infty)$, hence by selecting arbitrary values of y_1' the function $H(P_b, y_o', M_\infty)$ can be determined. Moreover, as will be seen later, I depends on y_o', M_∞, and H, so that the parametric structure of the equations ultimately yields the desired function $H(P_b, I, M_\infty)$.

The differential equation (3a) and the appropriate boundary conditions $y(0) = 0$, $y(s) = t/2$, and $y(s + l) = t/2$ determine x as a function of y by a single quadrature.

$$\sqrt{\lambda}\,x = \int \frac{\sqrt{\partial P/\partial y'}\,dy}{\sqrt{(t/2)^n - y^n}} = \begin{cases} \displaystyle\int_0^y \frac{\sqrt{\partial P/\partial y'}\,dy}{\sqrt{(t/2)^n - y^n}} & \text{on upstream surface} \\ \sqrt{\lambda}\,(s + l) + \displaystyle\int_{t/2}^y \frac{\sqrt{\partial P/\partial y'}\,dy}{\sqrt{(t/2)^n - y^n}} & \text{on downstream surface} \end{cases}$$

The algebraic sign to be selected for each radical is determined by the requirement that x increases as y increases on the upstream surface, and as y decreases on the downstream surface. The above relation is more conveniently expressed in terms of the dimensionless quantities $Y \equiv y/(t/2)$, $X \equiv x/s$, and $L \equiv l/s$. After eliminating $\sqrt{\lambda}$ by evaluating the above integral at $x = s$, there is obtained for the dimensionless shape

$$X = \begin{cases} \xi(Y) & \text{on upstream surface} \\ L + \xi(Y) & \text{on downstream surface} \end{cases} \tag{8}$$

where $\xi(Y)$ is defined as the quotient of two integrals[1]

$$\xi(Y) = \frac{\displaystyle\int_0^Y \sqrt{\partial P/\partial y'}\,dY/\sqrt{1 - Y^n}}{\displaystyle\int_0^1 \sqrt{\partial P/\partial y'}\,dY/\sqrt{1 - Y^n}} \tag{9}$$

The definite integral which normalizes $\xi(Y)$, such that $\xi(1) = 1$, will for sake of brevity be designated by j_n. Thus

$$j_n \equiv \int_0^1 \sqrt{\frac{\partial P}{\partial y'}}\,\frac{dY}{\sqrt{1 - Y^n}} \tag{10}$$

Actually, for completeness the function $\xi(Y)$ should be written as $\xi(Y; M_\infty, n, y_0')$ because it depends on the three quantities M_∞, n, and y_0' as well as the variable Y. For brevity, though, it is written simply as $\xi(Y)$.

Since x is a double-valued function of y over the chord length, $\xi(Y)$ is also a double-valued function of Y. A sketch of a typical curve of Y versus ξ is shown in figure 2. For a given dimensionless ordinate Y, one of the two values of ξ represents the dimensionless chordwise distance from the leading edge to a point on the upstream surface, whereas the other value represents (apart from an additive term L) the dimensionless chordwise distance from the leading edge to the point on the downstream surface which has the same ordinate Y. It is to be understood that in determining X from equation (8) the appropriate value of $\xi(Y)$ must be used for each surface; thus, for a given Y

[1]Since the integrands are singular at the point $Y = 1$, numerical computations of the function $\xi(Y)$ must allow for this singularity. A simple method of doing this is outlined in appendix A.

the value of $\xi(Y)$ appropriate to the downstream surface always is greater than for the upstream surface.

From the foregoing and the fact that $\xi(Y)$ is independent of P_b and σ, it follows that a curve of Y versus $\xi(Y)$, such as is illustrated in figure 2, determines the curved portions of an infinite number of optimum profiles, all having the same values of y_o', M_∞, and n. It may be noted that σ (equation (5)) essentially determines the length of straight midsection which is to be placed between the two curved portions after separating them at the point where $Y = 1$ (point AB in fig. 2); whereas P_b (equations (4) and (7)) essentially determines H, the value of Y beyond which the downstream portion of the curve is not used in a given case. It is noted that although the chord is fixed, the value of ξ corresponding to the trailing edge is not. This is because $\xi \equiv x/s$ changes whenever s changes.

As may be deduced from equation (7), y_1' determines H for a given n, M_∞, and y_o'. Moreover, y_1' determines P_b from equation (4). Hence, for any given value of base pressure the point on the downstream surface which corresponds to the trailing-edge position can be indicated on each $\xi(Y)$ curve. (See fig. 2 where the point corresponding to zero base pressure is indicated.)

Solution for L, $\bar{I}$, t/c, and s/c.- Turning now to the determination of the optimum length of straight midsection l, one sees from equation (5) that such a determination will also give $\bar{I}$. Since l is a function of y_o' and the given quantities n, σ, P_b, and M_∞, this enables y_o', the quantity used as a parameter in the present analysis, to be related to the quantity $\bar{I}$, which is a more convenient one to use if I is the actual quantity given. Starting with the definition of $\bar{I}$ the following equations result:

$$\bar{I} \equiv I/(t/2)^{n-\sigma}$$

$$= \frac{s}{c}\int_o^{c/s} Y^n \, dX = \frac{s}{c}\int_o^{c/s} [1 - (1 - Y^n)] \, dX$$

$$= \frac{s}{c}\left[\frac{c}{s} - \int_o^H (1 - Y^n)\frac{dX}{dY}\, dY\right]$$

or, by using the relation

$$\frac{dX}{dY} = \frac{1}{j_n}\sqrt{\frac{\partial P/\partial y'}{1 - Y^n}} \tag{11}$$

which follows from equations (8), (9), and (10), there results

$$\frac{1 - \bar{I}}{s/c} = \frac{1}{j_n}\int_o^H \sqrt{\frac{\partial F}{\partial y'}(1 - Y^n)}\, dY$$

For convenience the right-hand member of this equation is defined as $\eta(H)$.

$$\eta(H) \equiv \frac{1}{j_n}\int_0^H \sqrt{\frac{\partial P}{\partial y'}\left(1 - Y^n\right)}\, dY \tag{12}$$

From equations (8) and (5),

$$\frac{c}{s} = L + \xi(H)$$

$$= \frac{\sigma}{n}\frac{c}{s}\overline{I} + \xi(H)$$

Combining this with the above relation between $\overline{I}$ and s/c gives

$$\frac{s}{c} = \frac{n - \sigma}{n\xi(H) - \sigma\eta(H)} \tag{13}$$

and

$$\overline{I} = \frac{\xi(H) - \eta(H)}{\xi(H) - \frac{\sigma}{n}\eta(H)} \tag{14}$$

Recalling that H is determined by P_b for a given $\xi(Y)$ curve (given M_∞, n, y_o'), one sees that equation (14) determines $\overline{I}$ as a function of M_∞, n, σ, P_b, and y_o'. A convenient determination of $\overline{I}$, of course, can only be made if the function $\eta(H)$ in addition to $\xi(Y)$ has been computed. The function $\eta(H)$, which for completeness should be written as $\eta(H; M_\infty, n, y_o')$, is somewhat easier to compute than $\xi(Y)$ since it is not singular at $Y = 1$. Attention is called to the fact that all the above integrals with limits ranging from $Y = 0$ to $Y = H$, as in equation (12), for example, really correspond to integration over both curved surfaces, first from $Y = 0$ to $Y = 1$, and then from $Y = 1$ to $Y = H$.

With the position of maximum thickness determined by equation (13), the maximum thickness ratio can be determined in terms of the surface slope at the leading edge.

$$\left.\begin{aligned}\left(\frac{dY}{dX}\right)_o &= \frac{2s}{t}\left(\frac{dy}{dx}\right)_o \\ \frac{t}{c} &= 2\left(\frac{s}{c}\right)\frac{y_o'}{(dY/dX)_o}\end{aligned}\right\} \tag{15}$$

or, from equation (11), in an alternate form

$$\frac{t}{c} = 2\left(\frac{s}{c}\right)\frac{y_o'}{j_n}\sqrt{\left(\frac{\partial P}{\partial y'}\right)_o} \tag{15a}$$

Calculation of pressure drag of an optimum profile.- In reference 4 it was shown that for linearized supersonic airfoil theory the pressure

drag coefficient of an optimum profile was a simple algebraic function of certain quantities such as H and s/c. Since these quantities are known once the shape of the optimum profile is determined, a separate integration is not required in order to calculate the pressure drag. Fortunately, a similar algebraic relation can also be developed for the present case. In so doing, integration by parts is employed starting with the defining equation for pressure drag.

$$\frac{c}{2} c_d = \int_0^{h/2} P dy - P_b \frac{h}{2} = P_1 \frac{h}{2} - \int_{P_0}^{P_1} y dP - P_b \frac{h}{2} \tag{16}$$

In these equations, and subsequent ones, the integration is carried out only over the two curved portions since the straight midsection can contribute no drag. From equation (3a),

$$dP = \frac{\partial P}{\partial (1/y')} d\left(\frac{1}{y'}\right) = -y'^2 \frac{\partial P}{\partial y'} d\left(\frac{dx}{dy}\right)$$

$$= -\lambda \left[(t/2)^n - y^n\right] d\left(\frac{dx}{dy}\right)$$

hence, substituting into equation (16) and again integrating by parts gives

$$\frac{c}{2} c_d = \frac{h}{2}\left[P_1 - P_b + y_1' \left(\frac{\partial P}{\partial y'}\right)_1\right] - \lambda \int_0^s \left[(t/2)^n - (n+1)y^n\right] dx -$$

$$\lambda \int_{s+l}^{c} \left[(t/2)^n - (n+1)y^n\right] dx$$

The first bracketed term on the right side vanishes by virtue of equation (4). The remaining integrals can be simplified by noting that

$$\bar{I} = \frac{1}{c}\int_0^c \frac{y^n}{(t/2)^n} dx, \quad \frac{l}{c} = \sigma \frac{\bar{I}}{n}, \text{ and } \lambda (t/2)^n = y_0'^2 \left(\frac{\partial P}{\partial y'}\right)_0$$

There results

$$c_d = 2 y_0'^2 \left(\frac{\partial P}{\partial y'}\right)_0 \left[(n + 1 - \sigma)\bar{I} - 1\right] \tag{17}$$

This equation enables the pressure drag to be readily calculated if the base pressure is given, since P_b determines H for a given y_0' and M_∞, and H determines $\bar{I}$ in accordance with equation (14). Thus, equation (17) involves the base drag implicitly, but not explicitly. For the special case of linearized supersonic flow,

$$\frac{\partial P}{\partial y'} = 2/\sqrt{M_\infty^2 - 1}$$

and the above equation for c_d can be shown to reduce to the corresponding equation for pressure drag developed in reference 4.

Closed-Form Solution for the Special Case of Given Cross-Section Area $n = 1$, $\sigma = 0$

When the cross-section area of a profile is prescribed ($n = 1$, $\sigma = 0$), corresponding to a given wing volume, torsional stiffness, or torsional strength of a thin-skin structure, then the differential equation (3) can be integrated immediately with respect to x to yield a solution in closed form for the airfoil shape. There results

$$-\lambda x = P + y' \frac{\partial P}{\partial y'} + \text{constant} \tag{18}$$

The constants can be eliminated by evaluating this expression at $x = 0$ and $x = s$ to obtain

$$\frac{x}{s} \equiv X = \xi(Y) = 1 - \frac{P + y'(\partial P/\partial y') - P(0)}{P_0 + y_0'(\partial P/\partial y')_0 - P(0)} \tag{19}$$

Here $P(0)$ is the pressure coefficient at $y' = 0$, and P_0 is the pressure coefficient at $x = 0$. For practical purposes $P(0)$ usually can be taken as zero, although strictly speaking it should be regarded as a small quantity compared to $P_0 + y_0'(\partial P/\partial y')_0$. The parametric equations for Y and H in terms of y' are the same as before, only with $n = 1$.

$$Y = 1 - \frac{y'^2(\partial P/\partial y')}{y_0'^2(\partial P/\partial y')_0} \tag{20}$$

$$H = 1 - \frac{y_1'^2(\partial P/\partial y')_1}{y_0'^2(\partial P/\partial y')_0} \tag{21}$$

The general equation for the base pressure coefficient does not involve n, and hence is the same as before.

$$P_b = P_1 + y_1' \left(\frac{\partial P}{\partial y'}\right)_1 \tag{4}$$

The constant in equation (18) can be evaluated at $x = c$ instead of at $x = s$. Combining such an evaluation with the above equation for P_b yields the alternate expression

$$\frac{x}{c} = 1 - \frac{P + y'(\partial P/\partial y') - P_b}{P_0 + y_0'(\partial P/\partial y')_0 - P_b} \tag{22}$$

which involves P_b instead of $P(0)$. The equations for t/c, s/c, and c_d can be derived easily from the preceding equations. Omitting algebraic details, the following results are obtained:

By evaluating equation (18) at $x = c$, and combining with equations (3b) and (4),

$$\frac{t}{c} = \frac{2y_o'^2(\partial P/\partial y')_o}{P_o + y_o'(\partial P/\partial y')_o - P_b} \tag{23}$$

by evaluating equation (22) at $x = s$,

$$\frac{s}{c} = 1 - \frac{P(0) - P_b}{P_o + y_o'(\partial P/\partial y')_o - P_b} \tag{24}$$

and by substituting $n = 1$ and $\sigma = 0$ into equation (17),

$$c_d = 2\, y_o'^2 \left(\frac{\partial P}{\partial y'}\right)_o (2\bar{I} - 1) \tag{25}$$

Solution for the Special Case of Given Thickness Ratio $n = \infty$, σ = finite

In reference 4 it was shown that the limiting values $n = \infty$, σ = finite, represent the auxiliary condition of a given airfoil thickness ratio. The mathematical simplification inherent in the use of approximate theories such as linearized flow enables the solution for a given thickness ratio to be obtained directly by passing the general solution to the limit as $n \to \infty$. For shock-expansion theory, though, a general solution in closed explicit form cannot be obtained, and recourse to the alternate method indicated in reference 4 is required. This alternate method deals directly with the appropriate differential equation, which, for the case of given airfoil thickness, becomes simply

$$y'^2 \frac{\partial P}{\partial y'} = \text{constant} \tag{26}$$

which is satisfied by a profile composed of any number of straight segments. As shown in reference 4, the constant in the above equation does not change over the entire chord, with the result that the upper half of the profile forward of the trailing edge is composed of two straight lines, one extending from $x = 0 = y$ to $x = s$, $y = t/2$, and the other extending from $x = s$, $y = t/2$ to the trailing edge $x = c$, $y = h/2$. The slope is discontinuous at the point where $y = t/2$. To obtain a solution using any given airfoil theory, it is necessary to satisfy the differential equation (26), the end condition (4), and the boundary condition of a fixed thickness ratio.

Equation (17) for c_d becomes indeterminate as $n \to \infty$ because $\bar{I} \to 0$. For this case, however, the shape is known and the pressure drag can be determined from simple physical considerations:

$$(c_d)_{\text{given } t/c} = \frac{t}{c}\left[P_o - P_1(1 - H) - P_b H\right]$$

APPLICATION OF ANALYSIS

Flow at Infinite Mach Number

Prior to considering shock-expansion theory, the relatively simple case of flow at infinite Mach number over slender airfoils with small surface curvature will be considered. For such conditions the pressure coefficient on a surface facing upstream is proportional to the square of the local surface slope, that is, $P = Cy'^2$. Since the pressure coefficient is zero on any surface facing downstream it follows from physical considerations that $H = 1$. Equation (4) is satisfied by requiring that $y_1' = 0$. By consideration of the differential equation (3a) as specialized to the present case it follows that

$$\sqrt{\frac{\partial P}{\partial y'}} = \sqrt{2cy'} = (2c)^{1/3}\left[\lambda\left(\frac{t}{2}\right)^n\right]^{1/6}(1 - Y^n)^{1/6}$$

By substitution into equation (9), and employment of gamma functions to evaluate the integral in the denominator, there results

$$\xi(Y) = \frac{n\Gamma\left(\frac{2}{3} + \frac{1}{n}\right)}{\Gamma\left(\frac{2}{3}\right)\Gamma\left(\frac{1}{n}\right)}\int_0^Y (1 - Y^n)^{-1/3}dY \tag{27}$$

The function Y versus $\xi(Y)$ is plotted in figure 3 for $n = 1, 2, 3$, and ∞. The infinite value of n corresponds to the auxiliary condition of a given thickness ratio, and the optimum profile in this case is a wedge, since $\frac{1}{n}\Gamma\left(\frac{1}{n}\right) \to 1$ and $\xi(Y) \to Y$ as $n \to \infty$. It is seen that there is little difference between the three curves for finite n.

The other characteristic function needed for the complete determination of an optimum profile is $\eta(H)$. By substituting $H = 1$ in equations (12), (13), (14), and (17), and employing equations (5), (10), and (28), the following expressions are obtained:

$$\eta(1) = \frac{2n}{2n + 3} \tag{28}$$

$$\frac{s}{c} = \frac{(n - \sigma)(2n + 3)}{n(2n + 3 - 2\sigma)} \tag{29}$$

$$\overline{I} = \frac{3}{2n + 3 - 2\sigma} \tag{30}$$

$$\frac{l}{c} = \frac{3\sigma}{n(2n + 3 - 2\sigma)} \tag{31}$$

$$\frac{t}{c} = \frac{2}{c}\left(\frac{I}{\bar{I}}\right)^{\frac{1}{n-\sigma}} = \frac{2}{c}\left[\frac{(3 + 2n - 2\sigma)}{3} I\right]^{\frac{1}{n-\sigma}} \tag{32}$$

$$c_d = 4Cy_o'^3 \frac{(n - \sigma)}{(2n + 3 - 2\sigma)} \tag{33}$$

$$= 4C\left(\frac{t}{c}\right)^3 \left(\frac{c}{s}\right)^3 \left[\frac{\Gamma\left(\frac{2}{3}\right)\Gamma\left(\frac{1}{n}\right)}{2n\,\Gamma\left(\frac{2}{3} + \frac{1}{n}\right)}\right]^3 \frac{(n - \sigma)}{(2n + 3 - 2\sigma)} \tag{34}$$

If desired, this last equation for the pressure drag coefficient can be written in terms of I instead of t/c, inasmuch as I is related to the thickness ratio through equation (32). It should be noted that the above equations relate in closed form all pertinent properties of the optimum profile to the given quantities I, n, and σ. Examples of optimum profiles determined with the aid of these equations are presented subsequently.

Shock-Expansion Theory

When the oblique shock-wave and Prandtl-Meyer equations are combined to calculate the pressure on an airfoil surface in supersonic flow, the resulting equations for P are quite involved. The appropriate equation for $\partial P/\partial y'$, however, may be obtained by starting with the local differential relation

$$\frac{1}{\frac{1}{2}\rho V^2} \frac{\partial p}{\partial \delta} = \frac{2}{\sqrt{M^2 - 1}} \tag{35}$$

This point relation is formally the same as the corresponding relation applied throughout an entire flow field in linearized supersonic airfoil theory. The partial derivative $\partial p/\partial \delta$ is taken with M_∞ and δ_o held constant. Expressing equation (35) in terms of the pressure coefficient and free-stream conditions,

$$\frac{\partial P}{\partial \delta} = \frac{\rho V^2}{\rho_\infty V_\infty^2} \frac{2}{\sqrt{M^2 - 1}}$$

or, since

$$\frac{\partial P}{\partial y'} = \frac{\partial P}{\partial \delta} \cos^2 \delta$$

there results

$$\frac{\partial P}{\partial y'} = \frac{\rho V^2}{\rho_\infty V_\infty^2} \frac{2 \cos^2 \delta}{\sqrt{M^2 - 1}}$$

This equation appears fairly simple, but is not in a form which can be computed readily with the aid of existing tables where quantities such as local pressure ratio p/p_t and total-pressure ratio across a shock wave p_t/p_{t_∞} are tabulated. Thus, a more convenient form for calculating purposes is

$$\frac{\partial P}{\partial y'} = \frac{2}{\sqrt{M_\infty^2 - 1}} \left[\frac{M^2}{M_\infty^2} \sqrt{\frac{M_\infty^2 - 1}{M^2 - 1}} \frac{(p/p_t)}{(p_\infty/p_{t_\infty})} \left(\frac{p_t}{p_{t_\infty}} \right) \cos^2 \delta \right] \tag{36}$$

From this equation a numerical value of $\partial P/\partial y'$ can be determined from tabulated oblique-shock and expansion characteristics once y_o', M_∞, and the local slope y' are specified.

The functions $\xi(Y)$ and $\eta(H)$ have been calculated for shock-expansion theory by substituting equation (36) into equations (9) and (12), respectively, and then performing the indicated integration graphically by the method outlined in appendix A. In this process other useful quantities are calculated such as $(\partial P/\partial y')_o$ and j_n. The results are presented in figures 4, 5, 6, and 7. In figure 4 the quantity $(\partial P/\partial y')_o/(2/\sqrt{M_\infty^2 - 1})$, which is equal to $(\partial P/\partial y')_o/[(\partial P/\partial y')_o]_{\delta_o=0^o}$, is plotted as a function of δ_o for various values of M_∞. Similarly, $j_n/(j_n)_{\delta_o=0^o}$ is plotted in figure 5. It is to be noted

$$(j_n)_{\delta_o = 0^o} = \frac{2}{\sqrt{M_\infty^2 - 1}} \int_o^1 \frac{dY}{\sqrt{1 - Y^n}} = \frac{2k_n}{\sqrt{M_\infty^2 - 1}}$$

where

$$k_n = \begin{cases} 2 \text{ for } n = 1 \\ \pi/2 \text{ for } n = 2 \\ 1.4023\ldots \text{for } n = 3 \end{cases} \tag{37}$$

Curves of H^n versus δ_o for various values of base pressure are presented in figure 6, from which it is apparent that the dimensionless trailing-edge thickness increases if either the airfoil thickness increases (δ_o increases), or if the base pressure increases. In figure 7 the functions $\xi(Y)$ and $\eta(H)$ for various δ_o, M_∞, and n are presented plotted in the form Y versus ξ, and H versus η. The curves of Y versus ξ determine the shape of the optimum profile, while the curves of H versus η are useful in determining I, s/c, and t/c. Many of the curves of Y versus ξ have been terminated at the point (indicated by small circle) corresponding to zero base pressure.

EXAMPLES AND DISCUSSION

In order to determine an optimum profile it is necessary, of course, to know the base pressure. Experiments have shown that base pressure in two-dimensional flow depends principally on the Mach number, type of

boundary-layer flow, and the boundary-layer thickness at the base. (See reference 6.) Average experimental values are shown in figure 8 for both laminar and turbulent flow plotted as a function of the parameters proportional to the ratio of boundary-layer thickness to trailing-edge thickness. Step-by-step details of the method of determining an optimum profile by combining experimental base pressure data with the curves of figures 4 to 7 are given in appendix B.

In figure 9 examples of optimum profiles determined by the theory of the present report are shown together with corresponding profiles determined by linearized theory (reference 4). For each of the various auxiliary conditions the particular value of I selected for these examples is equal to that for a circular-arc biconvex airfoil of thickness ratio $t_{ca}/c = 0.06$. Since

$$I_{ca} = \frac{2^{2n}(n!)^2(t_{ca}/2)^{n-\sigma}}{(2n+1)!}$$

(see reference 4), it follows that with $c = 1$ the optimum profiles in figure 9 correspond to the value

$$I = \frac{2^{2n}(n!)^2(0.03)^{n-\sigma}}{(2n+1)!}$$

The auxiliary condition for $n = \infty$ (fig. 9(d)) corresponds to a given maximum airfoil thickness of 0.06c. As indicated in figure 9 (and also in subsequent figures of this report), the base pressure for $M_\infty = 1.5$ and $M_\infty = 3.0$ corresponds to turbulent boundary-layer flow at a Reynolds number of 10^7. Since h is involved in the abscissa of figure 8, due allowance is made for the variation of base pressure with trailing-edge thickness. Because base pressure data are not available as yet for $M_\infty = 8$, a constant value has been assumed ($p_b = 0.1\ p_\infty$) which is believed to be reasonable for a moderately thick trailing edge ($h/c \sim 0.05$ or more), but probably greatly overestimates the base drag for a thin trailing edge ($h/c \sim 0.01$ or less). For $M_\infty = \infty$, it is not necessary to know the base pressure since the optimum profile at this limit is independent of p_b.

In figure 10 examples are shown for various values of I with $M_\infty = 3$, $n = 3$, and $\sigma = 0$. Instead of specifying the value of I in each case, the thickness ratio of a structurally equivalent circular-arc biconvex airfoil is specified, as the significance of this latter value is easier to visualize. As would be expected, there is no appreciable difference between the profiles determined by linearized and shock-expansion theory when the value of I is small ($t_{ca}/c = 0.02$, for example), although differences are evident for larger values of I ($t_{ca}/c = 0.04$ and larger).

For each of the examples shown in figures 9 and 10, it is to be noted that in comparison to the profile determined by linearized theory, the corresponding optimum profile determined by shock-expansion theory

has a smaller slope over the portion of surface facing upstream, a position of maximum thickness farther aft, and a greater slope over the portion of surface facing downstream. This difference which increases with increasing Mach number is to be expected, as indicated in reference 4, because the linearized theory overestimates the suction forces and underestimates the positive pressure forces.

As regards drag coefficient, it is evident that drag calculations based on linearized theory cannot be used at hypersonic Mach numbers since the computed coefficient approaches zero as the Mach number increases. Also, it is to be remembered that linearized theory is considerably less accurate in predicting the drag of blunt-trailing-edge airfoils than of sharp-trailing-edge airfoils, since the Busemann second-order terms for the upstream and downstream surfaces do not cancel as they do when the trailing edge is sharp.

If shock-expansion theory is used to calculate the drag of the profile determined by linearized theory, the resulting value is only slightly greater than the drag of the same profile determined by shock-expansion theory. In order to put this idea on a more firm quantitative basis, the case of infinite Mach number can be considered, as the differences between profiles determined by linear and nonlinear theory are the greatest at this limit. (See examples in fig. 9.) By use of the expression $P = Cy'^2$ to calculate the drag of the profile determined by linear theory, and dividing by the drag calculated correspondingly for the profile determined by nonlinear theory, the following expression results:

$$\frac{\frac{k_n^2}{16(n+1)}\left[\frac{n+2-\sigma}{(n+2)(2n+3-2\sigma)}\right]^2}{\left[\frac{2(2n+3-2\sigma)}{3(n+2-\sigma)}\right]^{\frac{3}{n-\sigma}}}\left[\frac{2n(2n+3)\Gamma\left(\frac{2}{3}+\frac{1}{n}\right)}{\Gamma\left(\frac{2}{3}\right)\Gamma\left(\frac{1}{n}\right)}\right]^3 = \begin{cases} 1.08 \text{ for } n=1,\sigma=0 \\ 1.06 \text{ for } n=2,\sigma=0 \\ 1.07 \text{ for } n=2,\sigma=1 \\ 1.04 \text{ for } n=3,\sigma=0 \\ 1.05 \text{ for } n=3,\sigma=1 \\ 1.00 \text{ for } n=\infty,\sigma \text{ finite} \end{cases} \tag{38}$$

It is seen that at infinite Mach number the actual pressure drag of an optimum profile whose shape is determined by linearized theory does not exceed the drag of the true optimum profile by more than about 8 percent.

If consideration is given to the consistent differences noted earlier between the shapes of optimum profiles determined by linear and nonlinear theory, it is evident that linearized theory can be used with good accuracy to determine the optimum profile at any supersonic Mach number up to infinity.[2] Even without considering the consistent difference noted above, the profile determined by linearized theory is sufficiently accurate for most engineering purposes. Under less general conditions a similar

[2]As indicated in reference 4, however, the linearized theory does not yield a reasonably accurate profile at the low supersonic Mach numbers near or below shock detachment.

result also has been found in the recent investigation of Klunker and Harder (reference 7) which appeared while the present report was being prepared. The shape of some of the optimum profiles determined in reference 7, however, does not agree with the shape of analogous profiles in this report. For example, it is indicated in reference 7 that the profile of least drag for $t/c = 0.06$ has a sharp trailing edge at all Mach numbers below about 6, whereas the corresponding profiles shown in figure 9(d) indicate appreciable trailing-edge thickness even at Mach numbers of 1.5 and 3. This discrepancy is attributed to the arbitrary base pressure curve assumed in reference 7 which does not correspond to measured data for thin trailing edges.

From an engineering viewpoint it is desirable to know how much lower the drag of an optimum profile is than that of a sharp-trailing-edge profile, and also how much the optimum profile can be altered without significantly increasing the drag. In order to provide a basis of comparison, the zero-lift pressure drag of a family of sharp-trailing-edge circular-arc biconvex airfoils of various thickness ratios has been calculated by shock-expansion theory for the Mach number range between 1.5 and 8. The results are shown in figure 11. Thus, for any profile the drag of a structurally equivalent (same value of I) circular-arc biconvex profile can be determined readily from the curves in figure 11 by simply calculating t_{ca} from the equation

$$I = I_{ca} = 2^{2n}(n!)^2(t_{ca}/2)^{n-\sigma}/(2n + 1)!$$

Computations of drag have been made for a family of "semioptimum" profiles having arbitrarily selected values of trailing-edge bluntness H, a shape forward of the trailing edge that yields minimum foredrag for each particular H, and the same value of I as a circular-arc biconvex profile of thickness ratio t_{ca}. These calculations have been carried out for $t_{ca}/c = 0.02$, 0.04, 0.06, 0.08, and 0.10 at Mach numbers of 1.5, 3, and 8, and for various combinations of n and σ. As in previous examples, the base drag in each case was determined from the curves of figure 8 for turbulent-boundary-layer flow at $Re = 10^7$. The results are shown in figure 12 plotted in the form of a drag ratio versus H. Each curve corresponds to a constant value of I, and is identified by the thickness ratio (t_{ca}/c) of a circular-arc biconvex profile having the same value for I. In order to maintain a constant value of I, the actual thickness ratios (t/c) of the semioptimum profiles change somewhat as H varies between 0 and 1 (the ratio t/t_{ca} lies between about 0.90 and 1.05 for the case $n = 1$, $\sigma = 0$, between about 0.71 and 0.84 for $n = 2$, $\sigma = 1$, and between about 0.97 and 1.08 for $n = 3$, $\sigma = 0$). For each curve in figure 12 the semioptimum profile having the minimum drag coincides with the optimum profile determined from the curves of figures 5 to 8. The ordinate of each minimum point indicates the relative drag of the optimum compared to a structurally equivalent circular-arc biconvex profile, while the rise on each side of the minimum indicates the drag penalty resulting from the use of too much or too little trailing-edge thickness. It may be noted that some of the curves do not

cover the complete range of values of H. In all such cases, however, sufficient calculations were made so that the minimum point was bracketed.

Perhaps the most significant feature apparent from the curves of figure 12 is the large increase in drag that results for thin airfoils when a trailing-edge thickness considerably greater than the optimum is employed at moderate supersonic Mach numbers. The pressure drag of full-blunt profiles at Mach numbers of 1.5 and 3 for the case $t_{ca}/c = 0.02$ is several times the pressure drag of the optimum, the exact factor varying between about 2.8 and 3.9 depending on M_∞, n, and σ. On the other hand, for thicker profiles ($t_{ca}/c \approx 0.08$) the pressure drag is much less sensitive to variations in trailing-edge thickness about the optimum, and the use of a full-blunt profile instead of the optimum would result in a much smaller percent drag penalty. Also, for a given value of t_{ca}/c it is evident from figure 12 that the pressure drag becomes less sensitive to variations in trailing-edge thickness from the optimum as the Mach number is increased into the hypersonic regime.

As would be expected, the semioptimum sharp-trailing-edge profiles (H = 0 in fig. 12) have somewhat less pressure drag than a structurally equivalent circular-arc biconvex profile. The observed difference in drag for thin airfoils at moderate Mach numbers is negligible for the case of $n = 1$, $\sigma = 0$, since the optimum sharp-trailing-edge profile for these conditions is very close to a circular-arc biconvex profile (if linearized theory were employed the optimum sharp-trailing-edge profile for $n = 1$, $\sigma = 0$ would be a circular-arc biconvex profile). The corresponding difference in drag for the case $n = 2$, $\sigma = 1$, however, is significant since the optimum profile in this case has a midsection of constant thickness, and hence is of considerably different shape, as well as being considerably thinner than a structurally equivalent circular-arc biconvex profile.

Each of the curves for $M_\infty = 1.5$ and 3 (figs. 12(a) and 12(b)) show a minimum at some finite value of H, but the curves for $t_{ca}/c = 0.02$ at M = 8 (fig. 12(c)) do not. If all other parameters were constant, this trend would not be expected inasmuch as the optimum trailing-edge bluntness for a given thickness ratio generally increases as the Mach number is increased into the hypersonic range. (See reference 4.) The unexpected trend is observed in the present examples because the variation of base pressure with trailing-edge thickness is considered at M = 1.5 and 3 where experimental measurements are available, but it is not considered at $M_\infty = 8$ where, in the absence of experimental data, a constant base pressure was arbitrarily assumed (one-tenth of the free-stream pressure, irrespective of trailing-edge thickness). It is expected that if base pressure measurements were made at $M_\infty = 8$, they would show a dependence on trailing-edge thickness just as at the lower Mach numbers. Consequently, it is believed that the actual curves for the thinner airfoils at $M_\infty = 8$ will be greatly different than shown in figure 12(c), although the curves for the thicker airfoils are not expected to be significantly different. If a constant base pressure corresponding to measured values

on thick trailing edges were assumed at $M_\infty = 1.5$ and 3, the curves for $t_{ca}/c = 0.02$ would rise starting from $H = 0$ even more steeply than at $M_\infty = 8$. This illustrates the necessity of considering the dependence of base pressure on trailing-edge thickness in such an analysis.[3]

The drag of the various optimum profiles (minimum points in fig. 12) is seen to be less than the drag of a structurally equivalent circular-arc biconvex profile by amounts varying between about 1 percent and 53 percent, depending on the values of n, σ, M_∞, and t_{ca}/c. The largest drag reduction occurs for the case of $n = 2$, $\sigma = 1$, just as indicated by the linearized theory of reference 4. Likewise, the drag reduction generally increases as the Mach number or the thickness ratio is increased, as predicted by linearized theory.

CONCLUSIONS

1. For a given Mach number and structural requirement, the shape and drag of the profile having the least possible pressure drag at zero lift, as computed from shock-expansion theory, can be determined readily provided the base pressure is known from experiments and provided curves of certain characteristic functions are available. (These functions are $\xi(Y, \delta_o, n)$, $\eta(H, \delta_o, n)$, $H(\delta_o, p_b/p_\infty, n)$, $j_n(\delta_o)$, and $\partial P/\partial y'$ (δ_o), examples of which are presented in figures 4 to 7.)

2. A comparison of profiles determined by shock-expansion theory and linearized theory indicates that the linearized theory may be used with reasonable accuracy at Mach numbers up to infinity to determine the shape of the optimum profile, although it can be used only at moderate supersonic Mach numbers to determine the drag.

3. Considerable deviations in profile shape from the theoretical optimum can be made without increasing the drag excessively provided the Mach number is high, or the airfoil thickness ratio is relatively large. Large drag penalties result, however, if a trailing-edge thickness appreciably greater than the optimum is employed on a thin airfoil at moderate supersonic Mach numbers.

4. It is necessary to consider the experimentally observed dependence of base pressure on trailing-edge thickness when calculating the optimum-profile shape and drag of a thin airfoil.

Ames Aeronautical Laboratory
National Advisory Committee for Aeronautics
Moffett Field, Calif., June 25, 1952

[3]If the boundary layer were laminar, the effect on the optimum shape of the dependence of base pressure on trailing-edge thickness would be even greater.

APPENDIX A

METHOD OF CALCULATING $\xi(Y)$

The singularity at $Y = 1$ of the integrands in equation (9) causes difficulty when directly evaluating such integrals numerically or graphically. This difficulty, however, can be circumvented by transforming from Y as the integration variable to a new function $f_n(Y)$ defined as follows:

$$f_n(Y) \equiv \int_0^Y \frac{dY}{\sqrt{1 - Y^n}} \tag{A1}$$

With this transformation the equation for $\xi(Y)$ becomes

$$\xi(Y) = \frac{\int_0^{f_n(Y)} \sqrt{\frac{\partial P}{\partial y'}}\, df_n}{\int_0^{k_n} \sqrt{\frac{\partial P}{\partial y'}}\, df_n} \tag{A2}$$

In this equation the integrands and the ranges of integration are all finite. The constant k_n is the same quantity as that used in reference 4, namely,

$$k_n = f_n(1) = \left\{ \begin{array}{ll} 2 & \text{for } n = 1 \\ \pi/2 & \text{for } n = 2 \\ 1.4023 & \text{for } n = 3 \\ 1 & \text{for } n = \infty \end{array} \right\} \tag{A3}$$

The functions $f_n(Y)$, apart from an additive constant, are likewise the same characteristic functions as appeared throughout the analysis of reference 4 when linearized supersonic airfoil theory was employed for P. Thus,

$$f_n(Y) = \left\{ \begin{array}{ll} 2\left(1 - \sqrt{1 - Y^n}\right) & \text{for } n = 1 \\ \sin^{-1} Y & \text{for } n = 2 \\ 1.4023 - 3^{-\frac{1}{4}} F(k, \varphi) & \text{for } n = 3 \\ Y & \text{for } n = \infty \end{array} \right\} \tag{A4}$$

where $F(k,\varphi)$ is the incomplete elliptic integral of the first kind of modulus $k = \sin 75^\circ = 0.9659$, and amplitude

$$\varphi = \cos^{-1} \frac{(\sqrt{3} - 1 + Y)}{(\sqrt{3} + 1 - Y)}$$

With the transformation to f_n, the integrals in equation (A2) are evaluated by first selecting a number of values of y' ranging from y_o' to large negative values. For each y' the ordinate Y is computed from equation (6), f_n from equation (A4), and $\partial P/\partial y'$ from the particular airfoil theory. A plot is then made of $\partial P/\partial y'$ versus f_n in order to evaluate the integrals determining $\xi(Y)$.

APPENDIX B

DETAILS OF METHOD OF DETERMINING THE SHAPE AND DRAG OF AN OPTIMUM PROFILE BY SHOCK-EXPANSION METHOD

In the shock-expansion equations the leading-edge deflection angle δ_o is a more convenient parameter to use than the given value of I, hence the steps outlined below involve an iterative procedure.

(1) Assume values of δ_o and p_b/p_∞

(2) Read value of H^n from figure 6 and compute H

(3) Read values of $\xi(H)$ and $\eta(H)$ from figure 7; compute $\bar{I}$ from equation (14) and s/c from equation (13)

(4) Read value of $(\partial P/\partial y')_o$ from figure 4, $j_n/(j_n)_{\delta_o = 0^o}$ from figure 5; compute $(j_n)_{\delta_o = 0^o}$ from equation (37), t/c from equation (15a)

(5) Compute $I = \bar{I}\,(t/2)^{n-\sigma}$

By comparison of the computed value of I with the given value, a new value of δ_o can be estimated. Also, from the computed value of h/c, the experimental base pressure curves in figure 8 yield a new value of p_b/p_∞. By repetition of the above steps until the final computed value of I is equal to the given value, and the final computed value of h/c corresponds to the final base pressure assumed, all characteristics (δ_o, t/c, s/c, H, $\xi(Y)$, $(\partial P/\partial y')_o$, j_n, and $\bar{I}$) of the optimum profile are determined. The pressure drag is then calculated from equation (17).

REFERENCES

1. Saenger, Eugen: Raketen-Flugtechnik. R. Oldenbourg, Munchen und Berlin, 1933.

2. Ivey, H. Reese: Notes on the Theoretical Characteristics of Two-Dimensional Supersonic Airfoils. NACA TN 1179, 1947.

3. Smelt, R.: Problems of Missiles at Extreme Speeds. NOLR 1131, Symposium on Ordnance Aeroballistics, June 1949, pp. 51-68.

4. Chapman, Dean R.: Airfoil Profiles for Minimum Pressure Drag at Supersonic Velocities - General Analysis and Application to Linearized Supersonic Flow. NACA TN 2264, 1951.

5. Eggers, A. J., Jr., and Syvertson, Clarence A.: Inviscid Flow About Airfoils at High Supersonic Speeds. NACA TN 2646, 1952.

6. Chapman, Dean R., Wimbrow, William R., and Kester, Robert H.: Experimental Investigation of Base Pressure on Blunt-Trailing-Edge Wings at Supersonic Velocities. NACA TN 2611, 1952.

7. Klunker, E. B., and Harder, Keith C.: Comparison of Supersonic Minimum-Drag Airfoils Determined by Linear and Nonlinear Theory. NACA TN 2623, 1952.

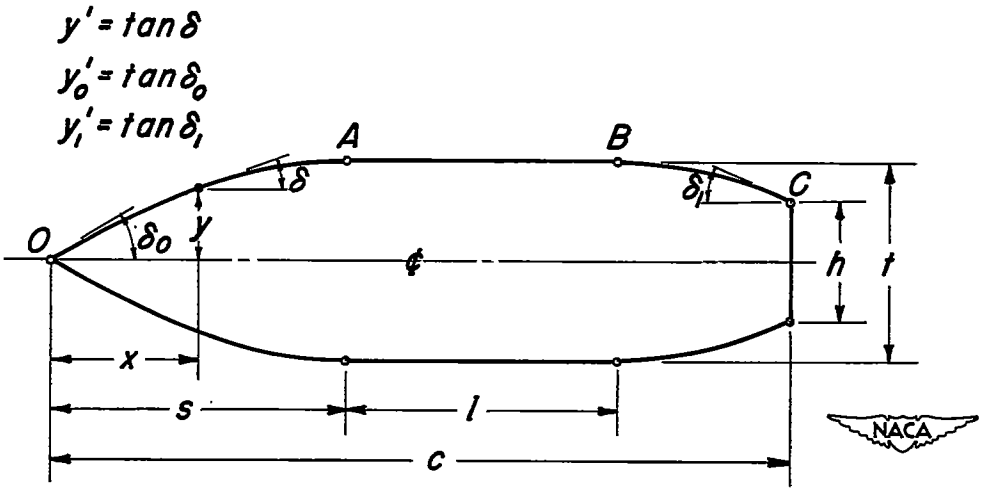

Figure 1.- Sketch illustrating various symbols used in the analysis.

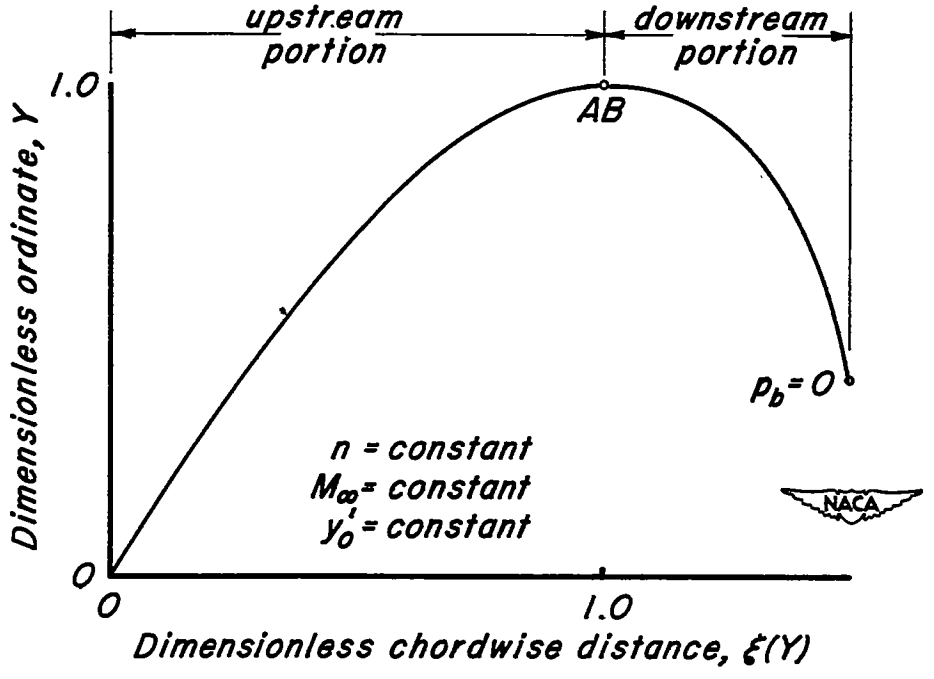

Figure 2.- Sketch of a typical curve for determining optimum-airfoil profiles.

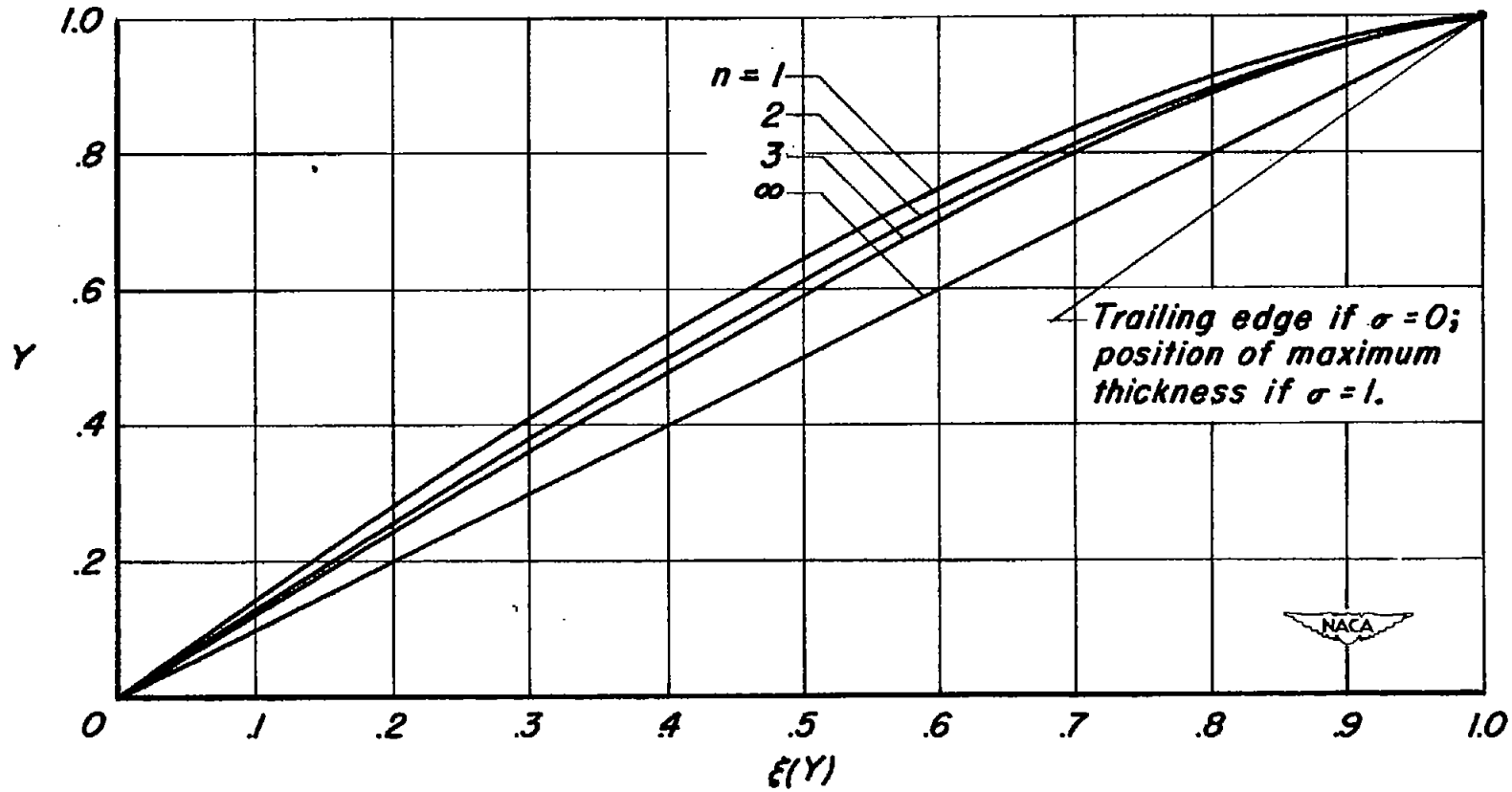

Figure 3.- Characteristic curves applicable to the simplified equation for flow at infinite Mach number.

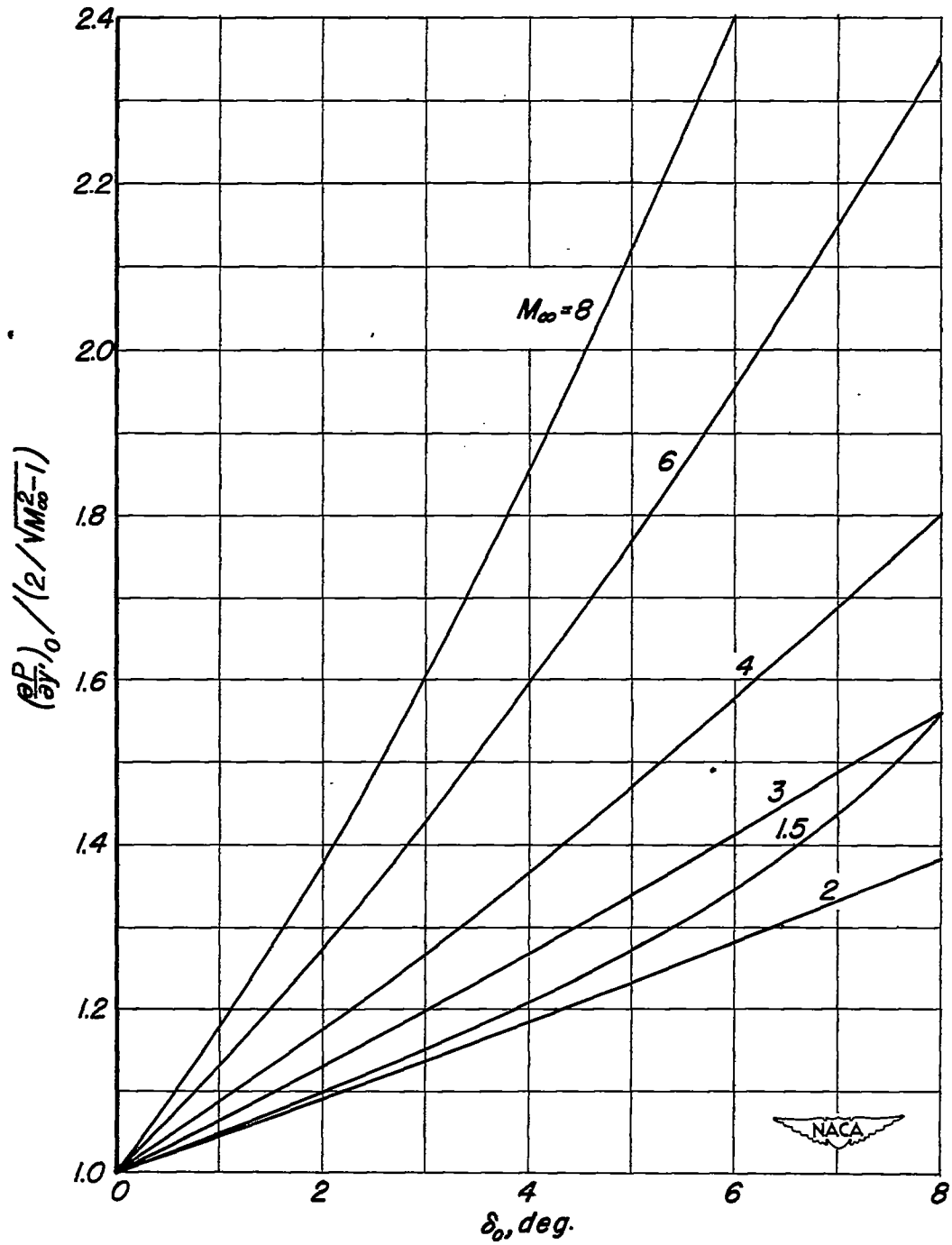

Figure 4.– Curves based on shock-expansion theory showing $\left(\frac{\partial P}{\partial y'}\right)_0 / \left(2/\sqrt{M_\infty^2-1}\right)$ *as a function of leading-edge deflection angle for various Mach numbers.*

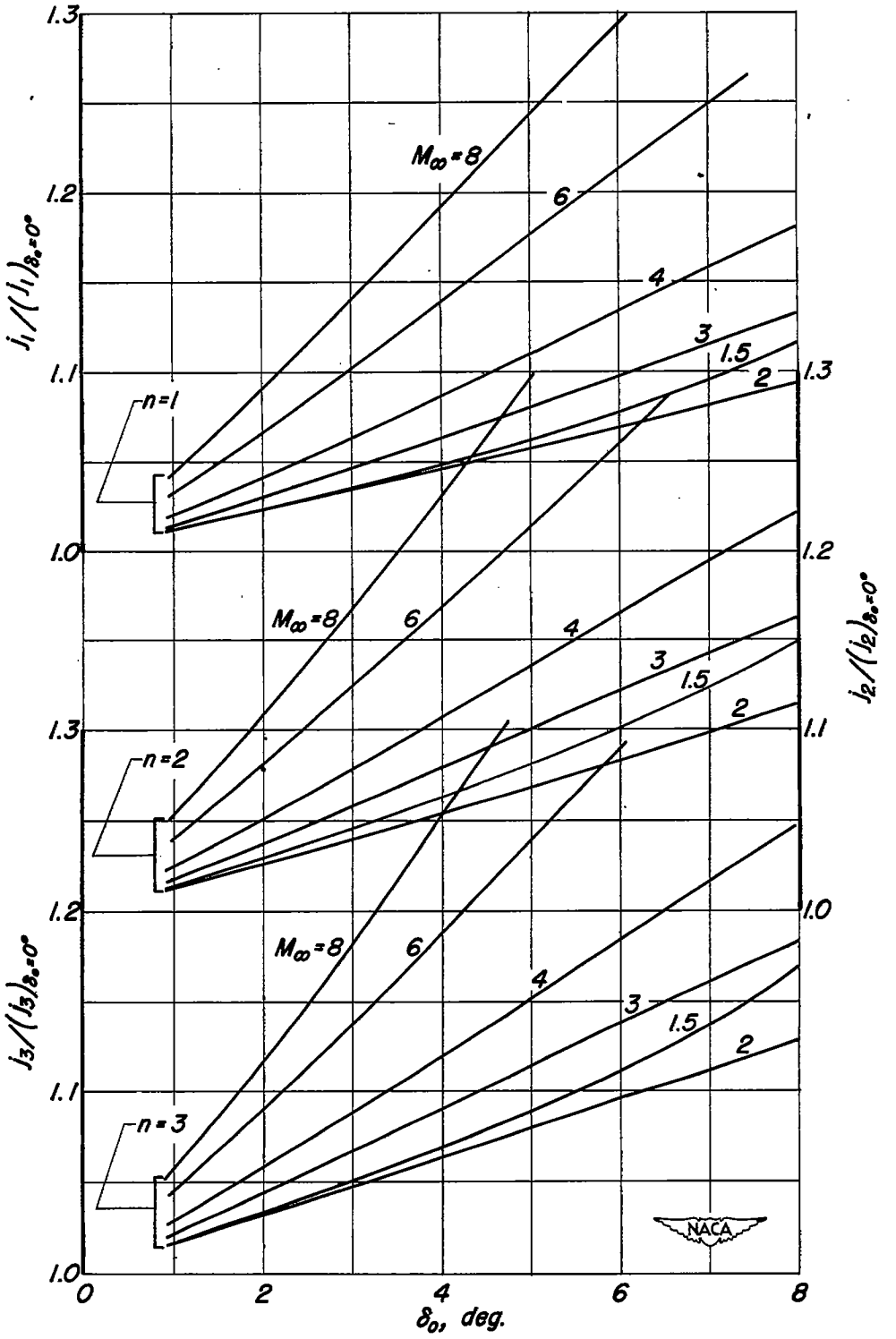

Figure 5.—Curves based on shock-expansion theory showing $j_n/(j_n)_{\delta_0=0°}$ as a function of leading-edge deflection angle for various Mach numbers.

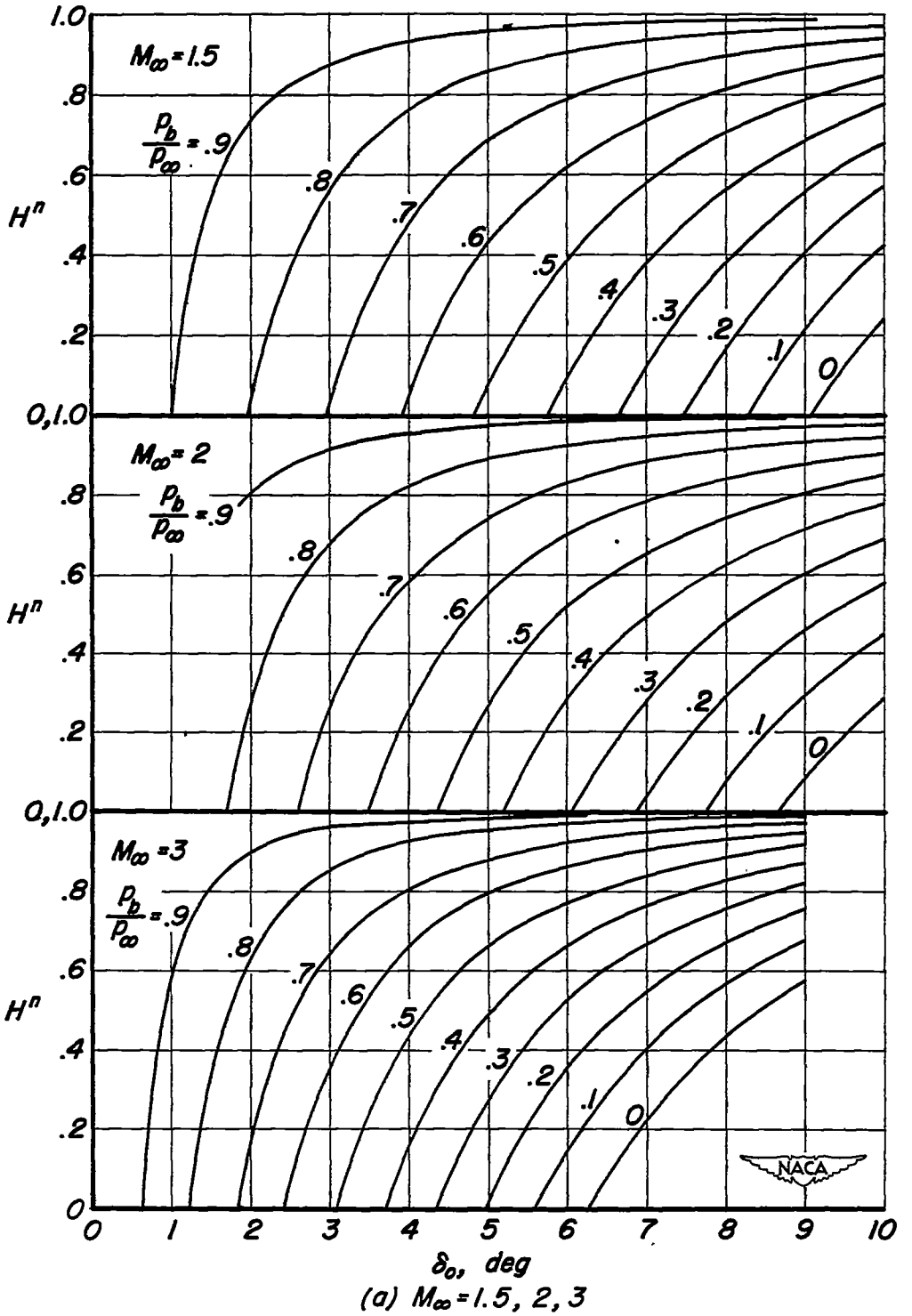

(a) $M_\infty = 1.5, 2, 3$

Figure 6.—Curves based on shock-expansion theory showing dimensionless trailing-edge thickness as a function of base pressure and leading-edge deflection angle.

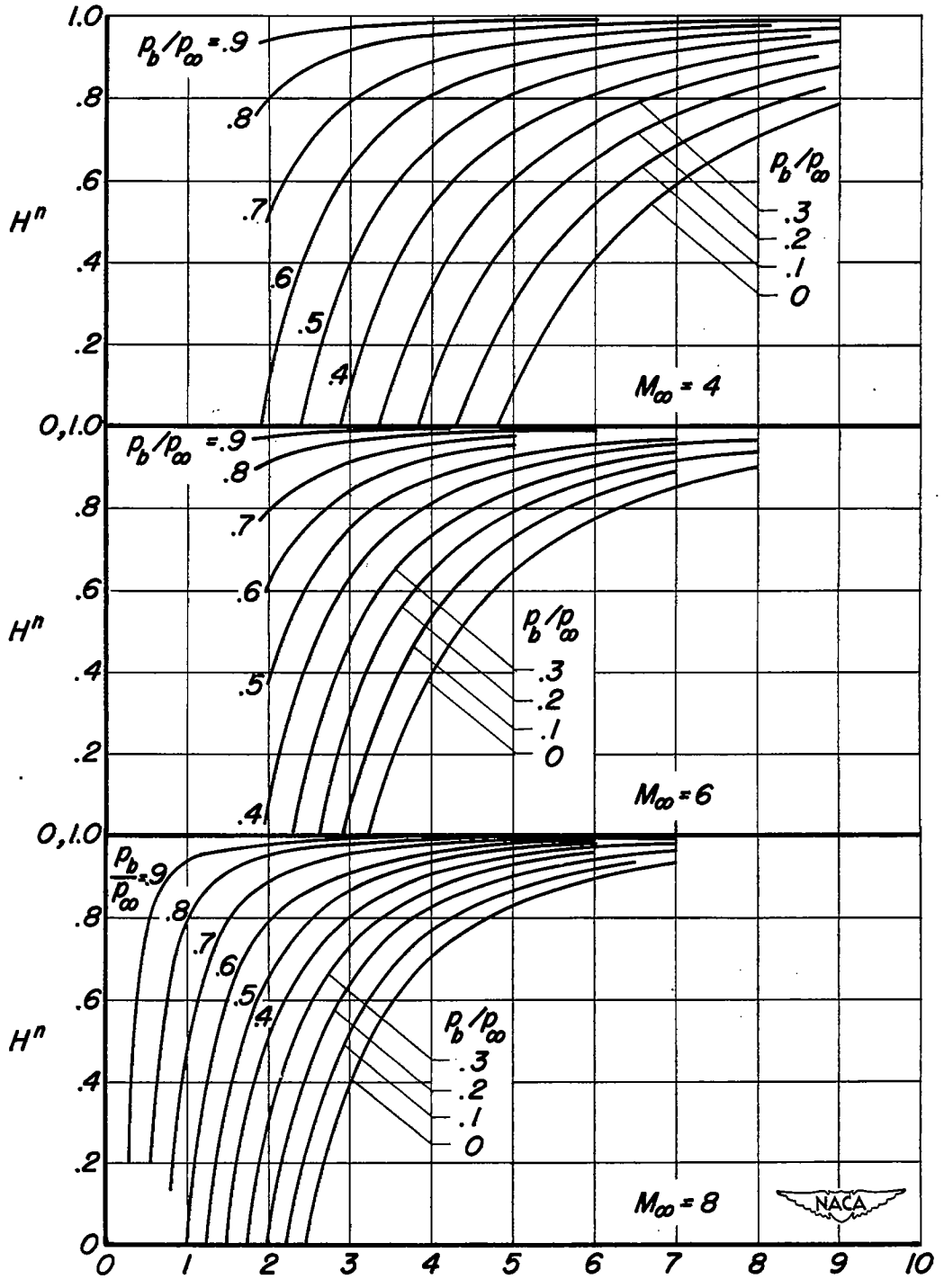

(b) M_∞ = 4, 6, 8

Figure 6.— Concluded.

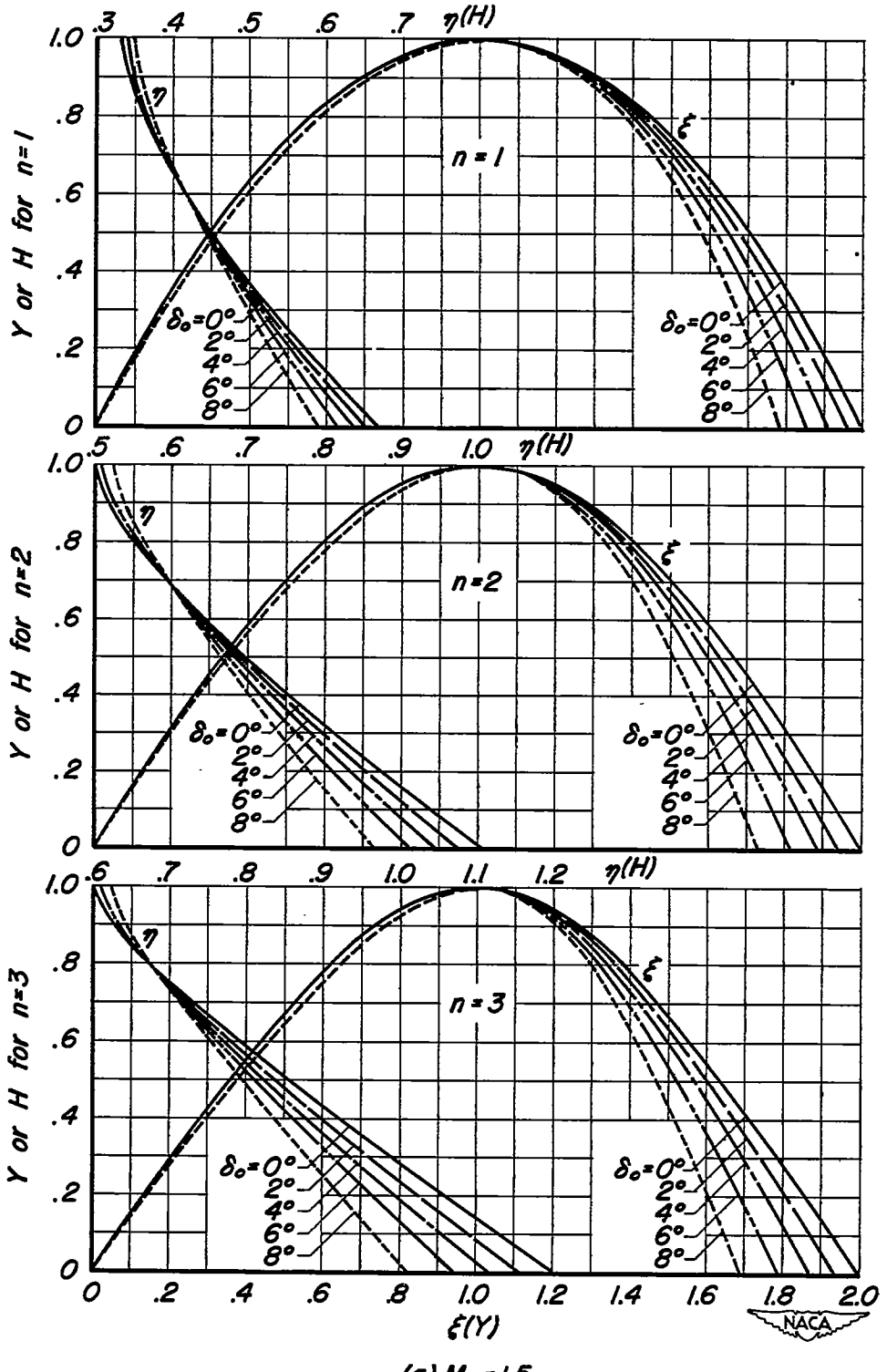

(a) $M_\infty = 1.5$

Figure 7.—Curves based on shock-expansion theory showing Y as a function of ξ and H as a function of η for various values of n and δ_o.

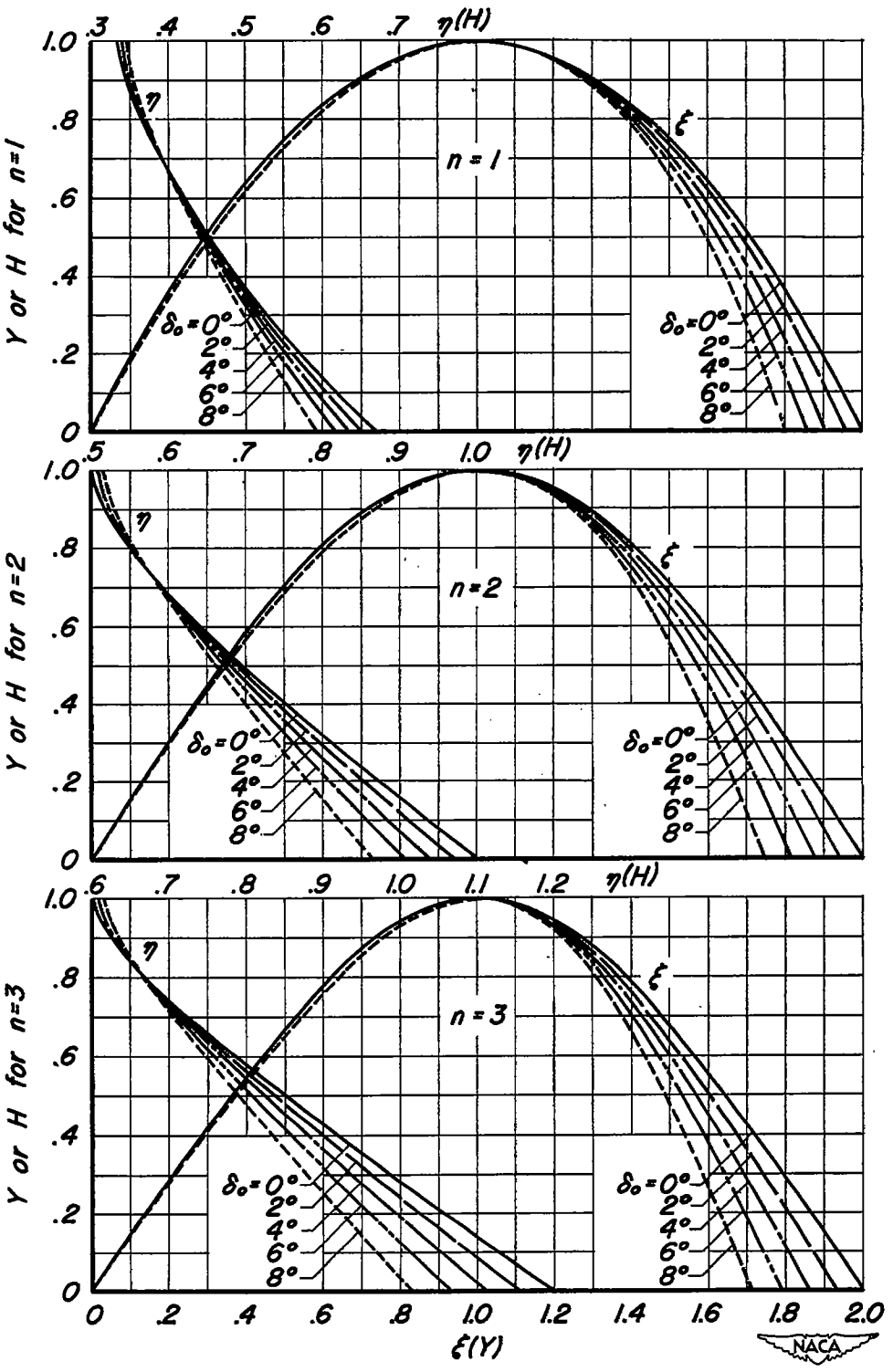

(b) $M_\infty = 2$

Figure 7.– Continued.

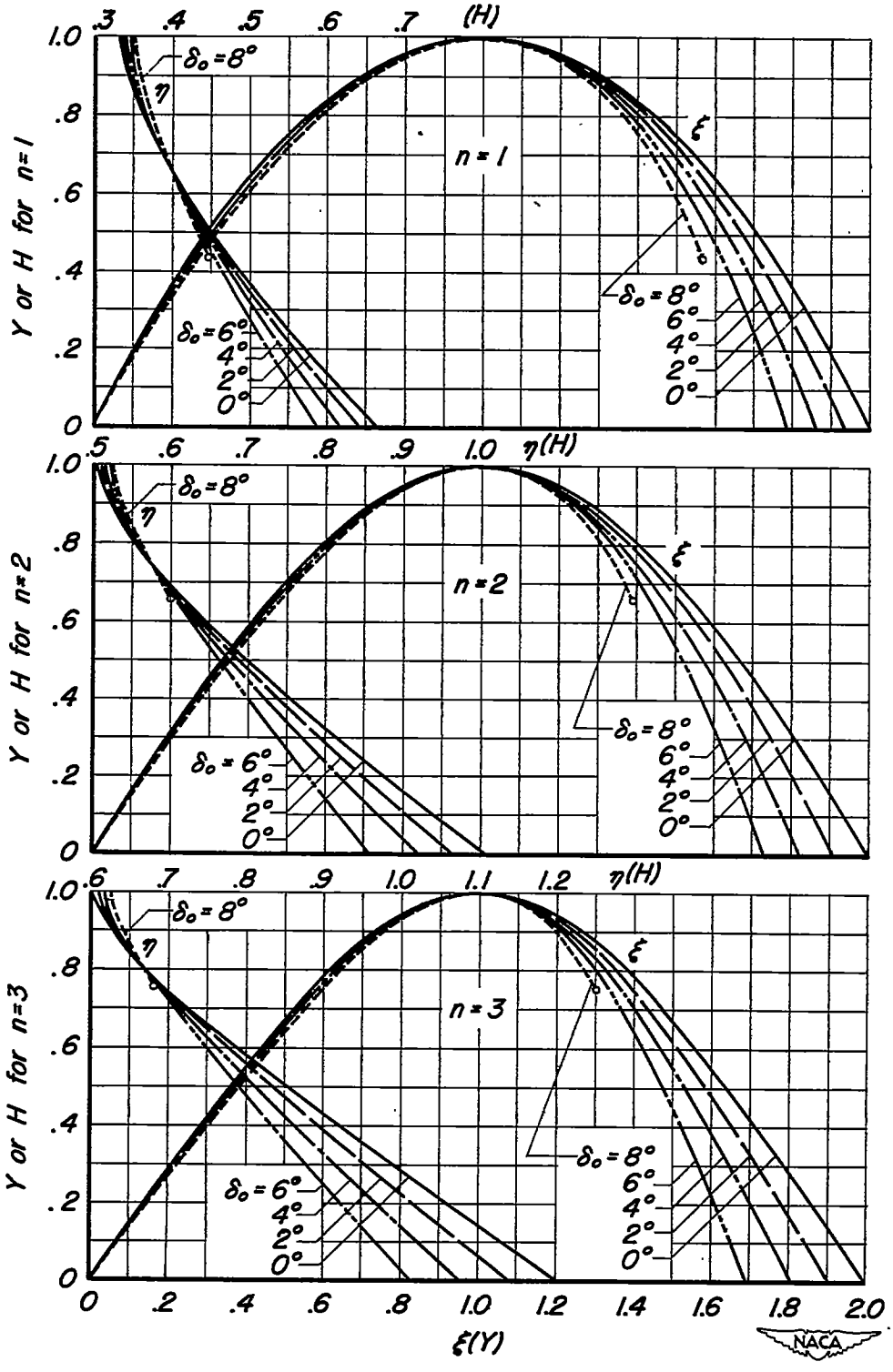

(c) $M_\infty = 3$

Figure 7.—Continued.

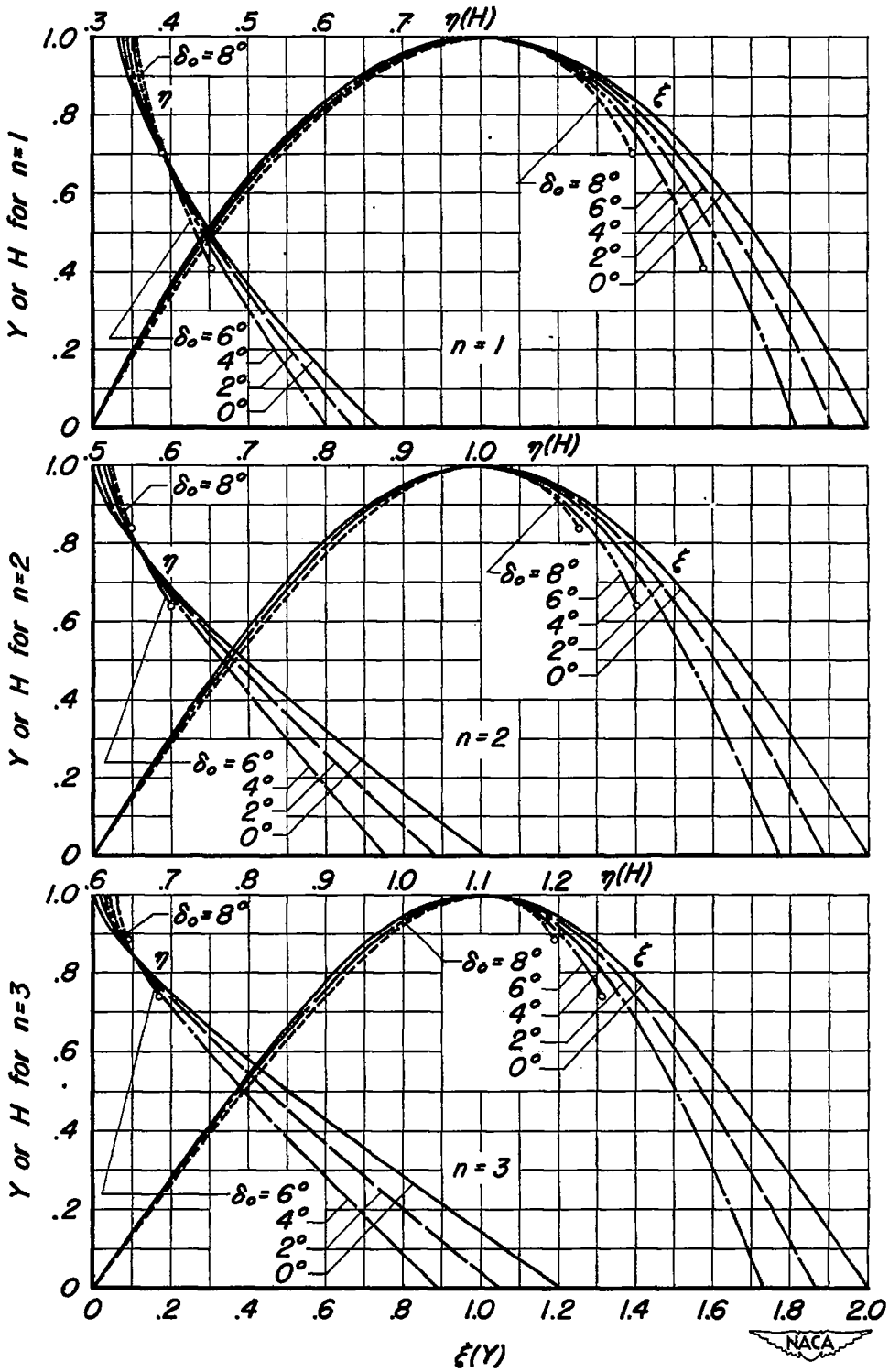

(d) $M_\infty = 4$

Figure 7.—Continued.

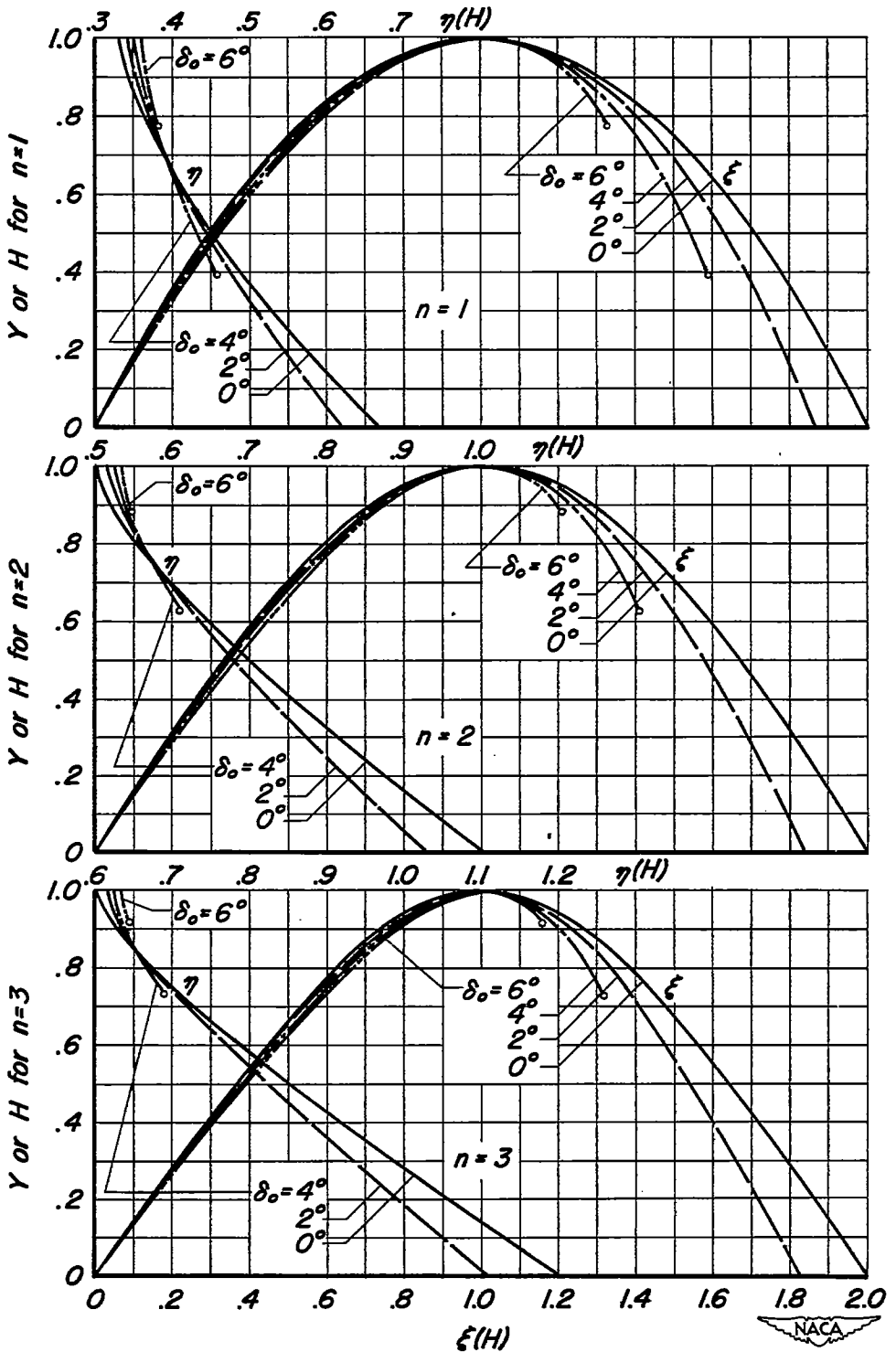

(e) $M_\infty = 6$

Figure 7. — Continued.

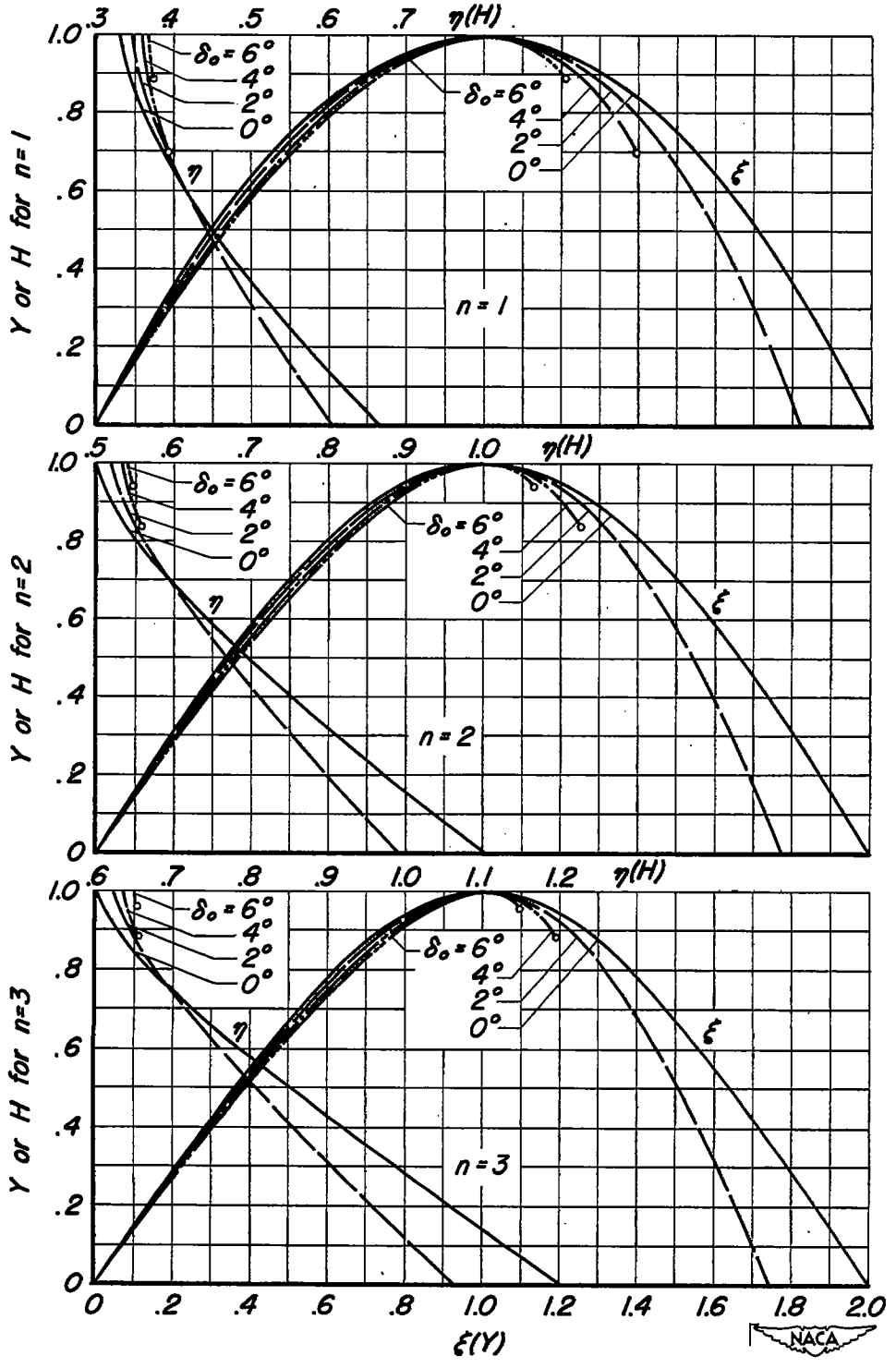

(f) $M_\infty = 8$

Figure 7. —Concluded.

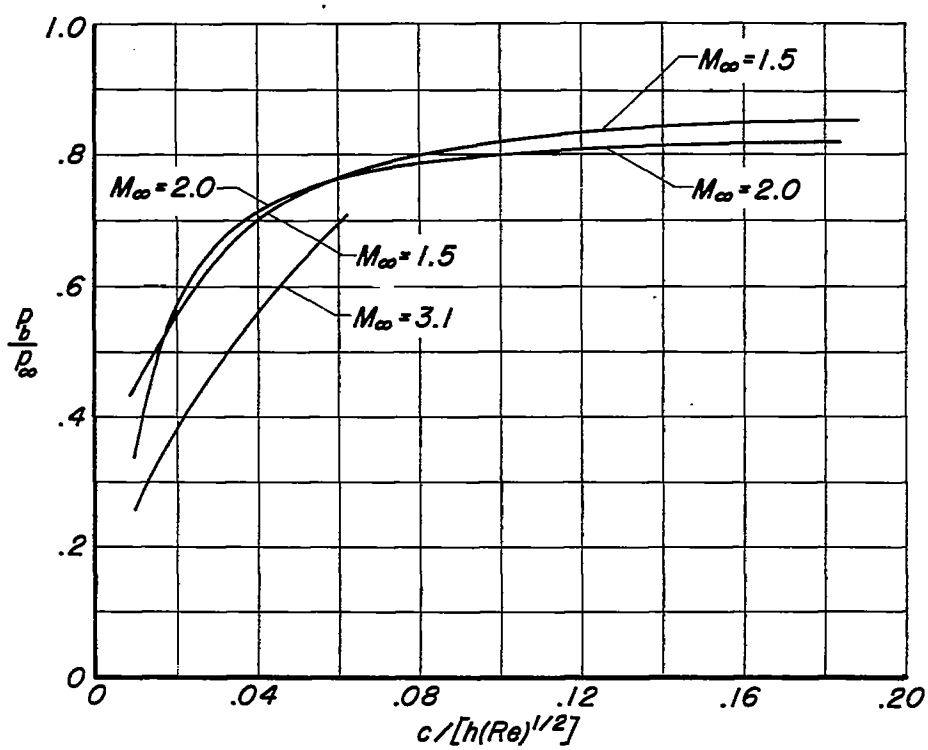

(a) Laminar flow

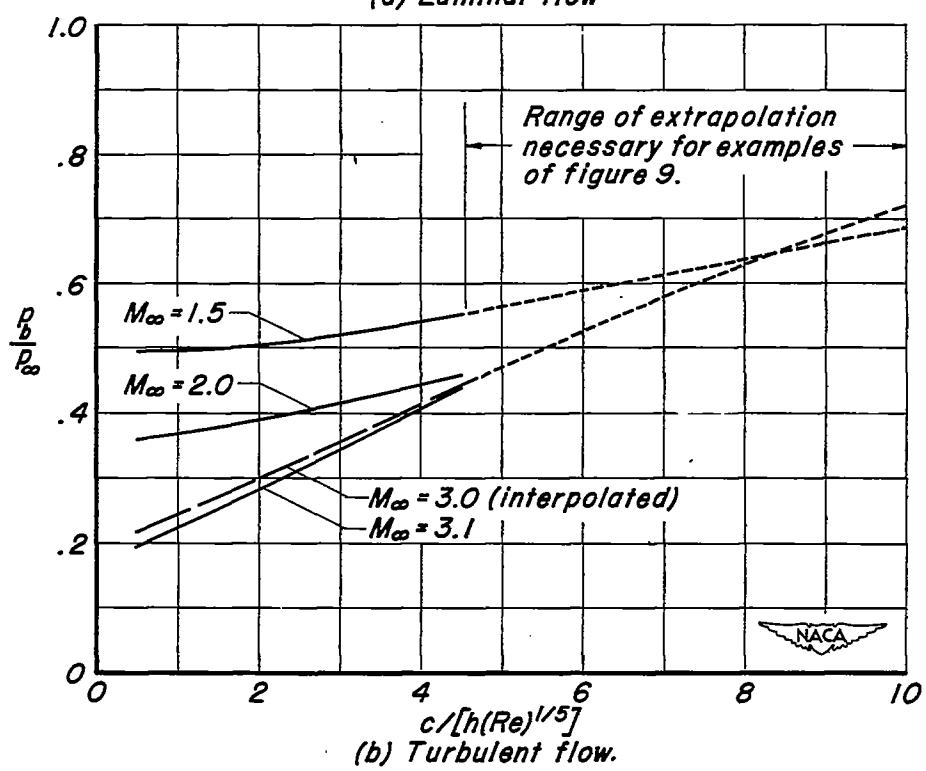

(b) Turbulent flow.

Figure 8.- Average experimental values of base pressure from reference 6.

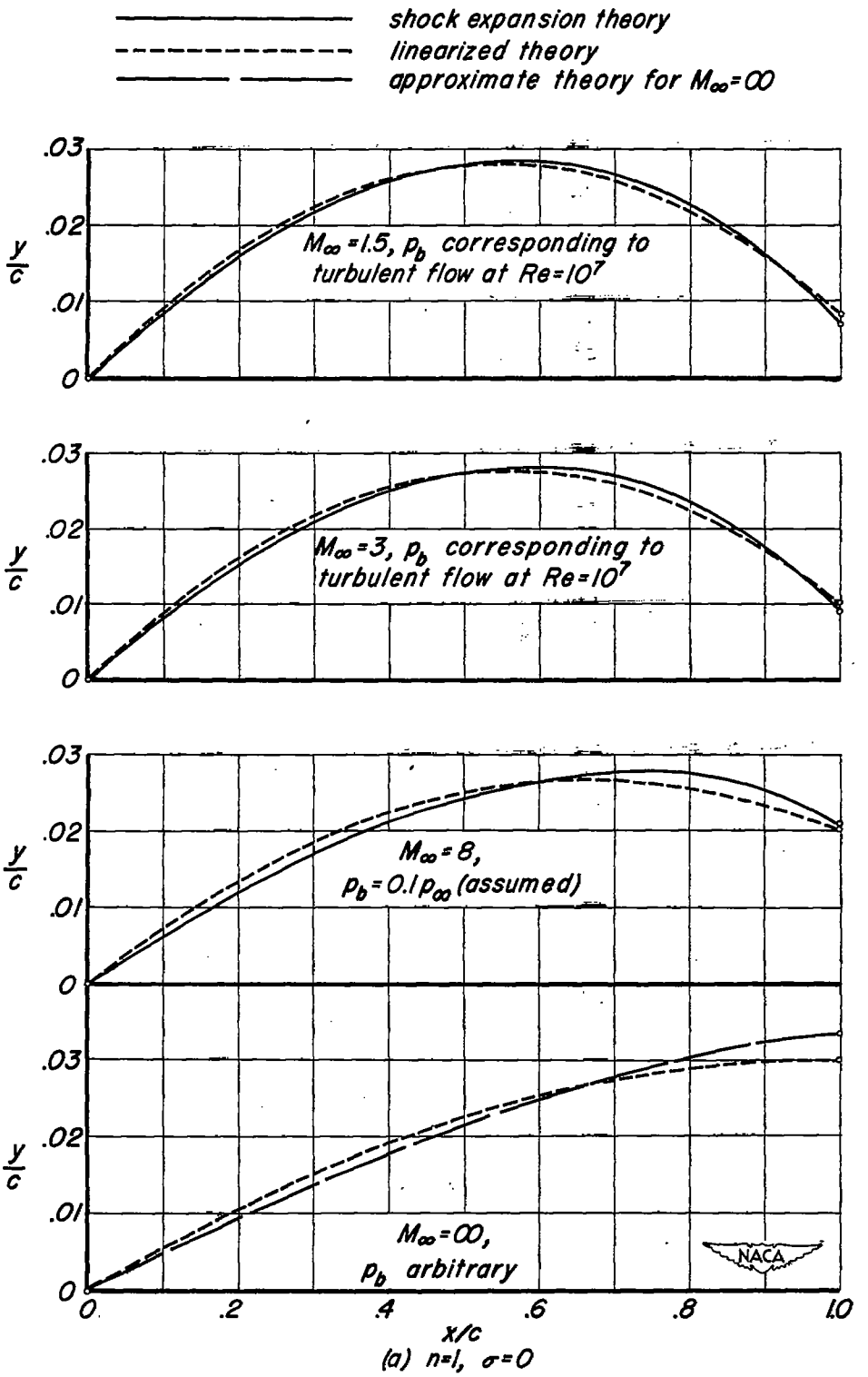

(a) $n=1$, $\sigma=0$

Figure 9.- Examples of optimum profiles; auxiliary integral equal to that of a circular-arc biconvex airfoil of thickness ratio 0.06.

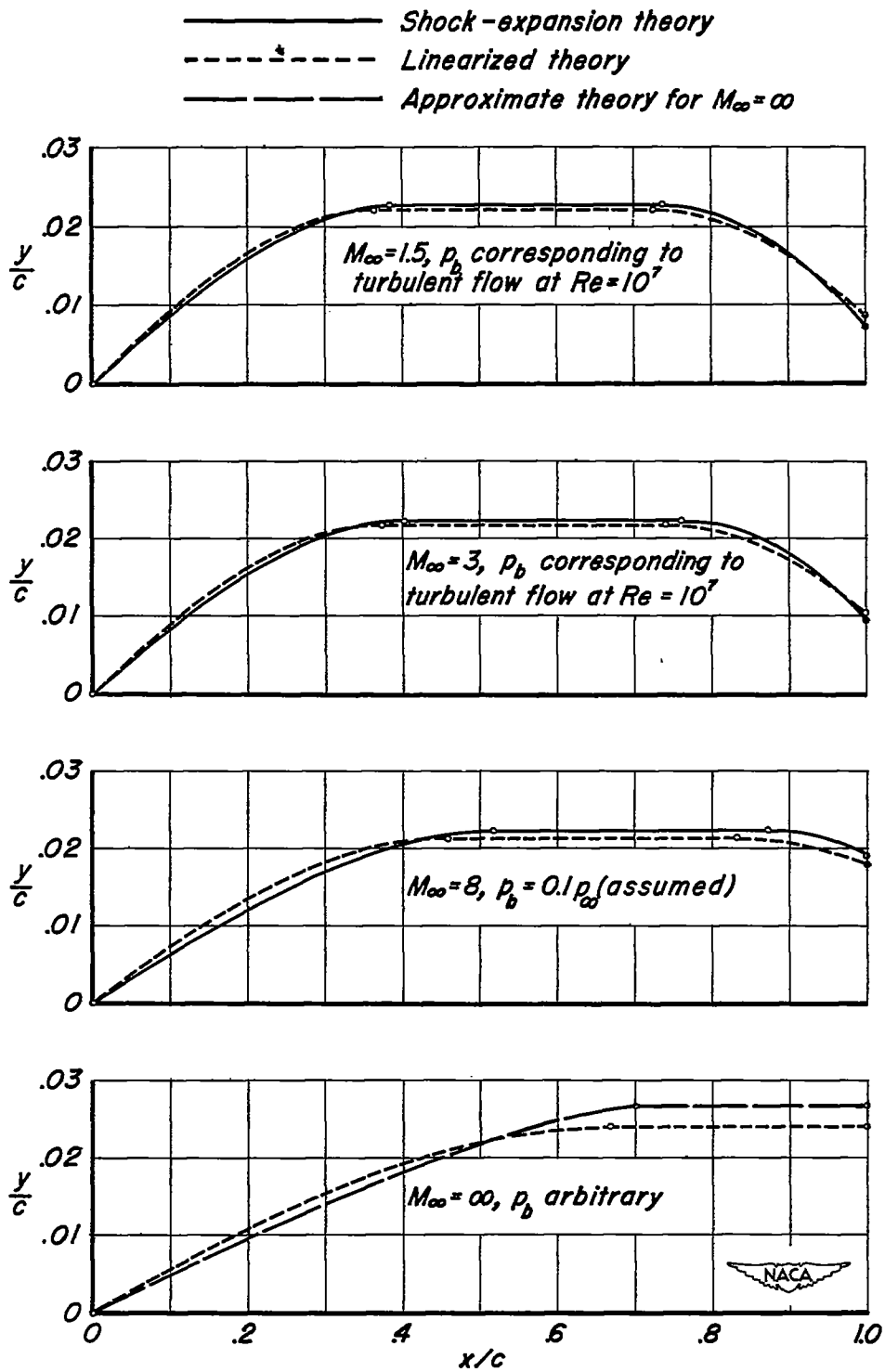

(b) $n = 2$, $\sigma = 1$

Figure 9.– Continued.

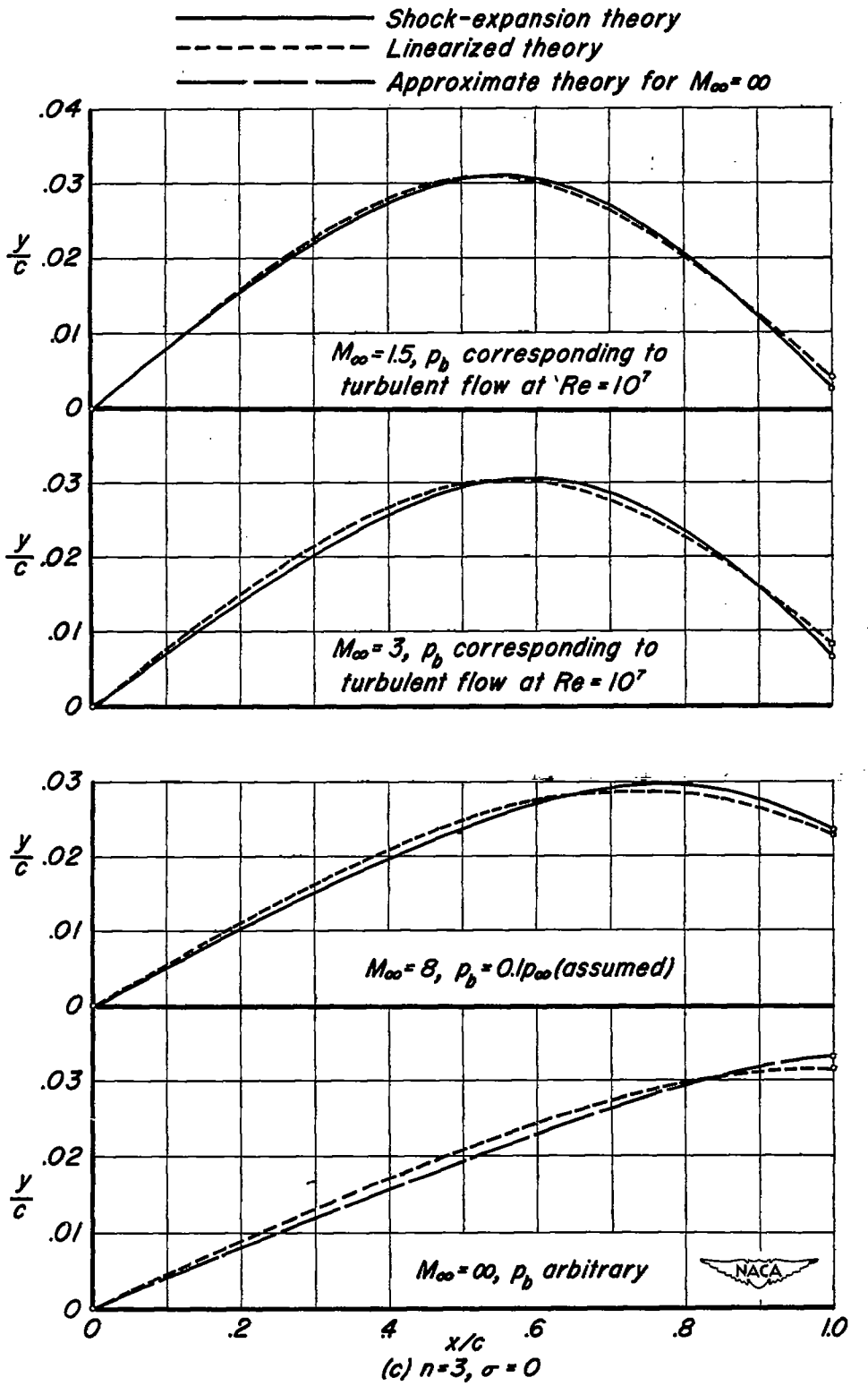

(c) $n = 3$, $\sigma = 0$

Figure 9.– Continued.

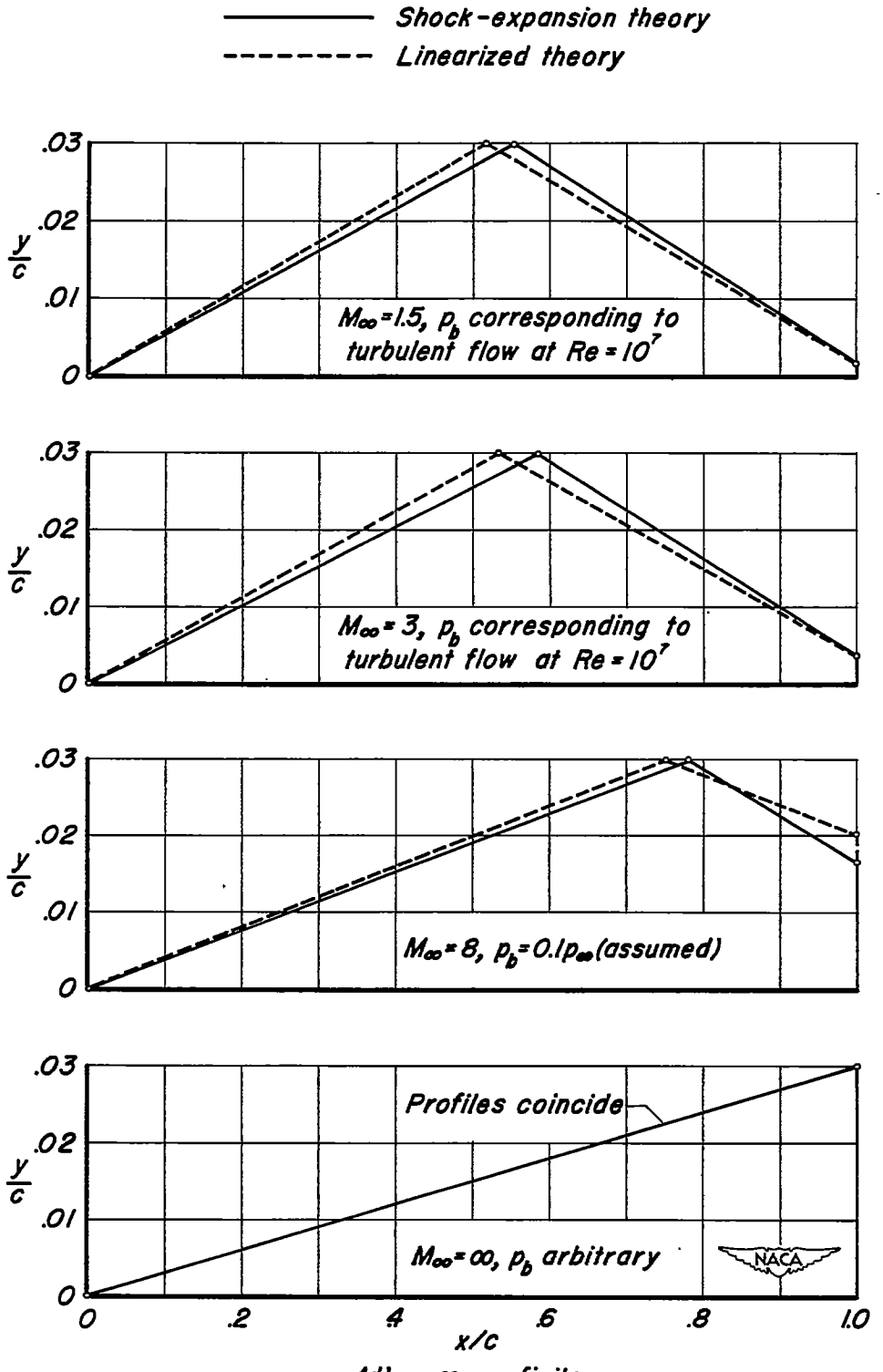

(d) $n=\infty$, σ = finite

Figure 9.- Concluded.

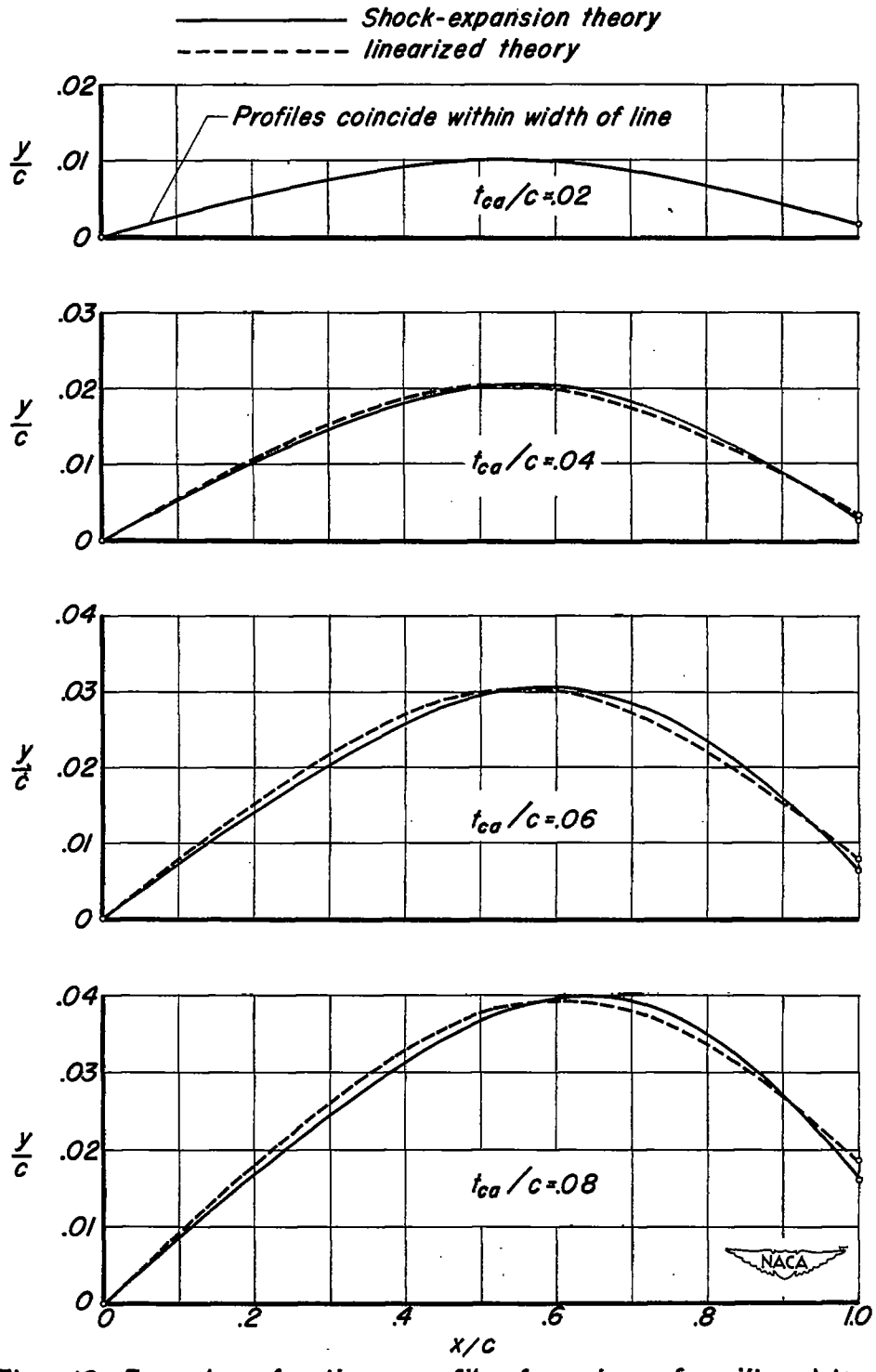

Figure 10.– Examples of optimum profiles for values of auxiliary integral equal to that of a circular-arc biconvex airfoil of maximum thickness t_{ca}; $n = 3$, $\sigma = 0$; $M_\infty = 3$; base pressure corresponding to turbulent flow at $Re = 10^7$.

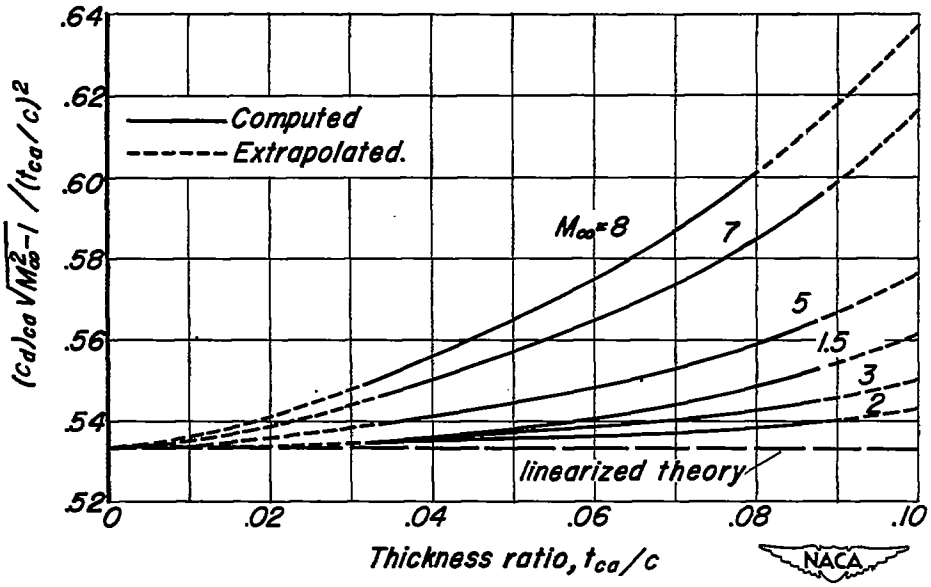

Figure 11.-Pressure drag of circular-arc biconvex airfoils determined by shock-expansion theory.

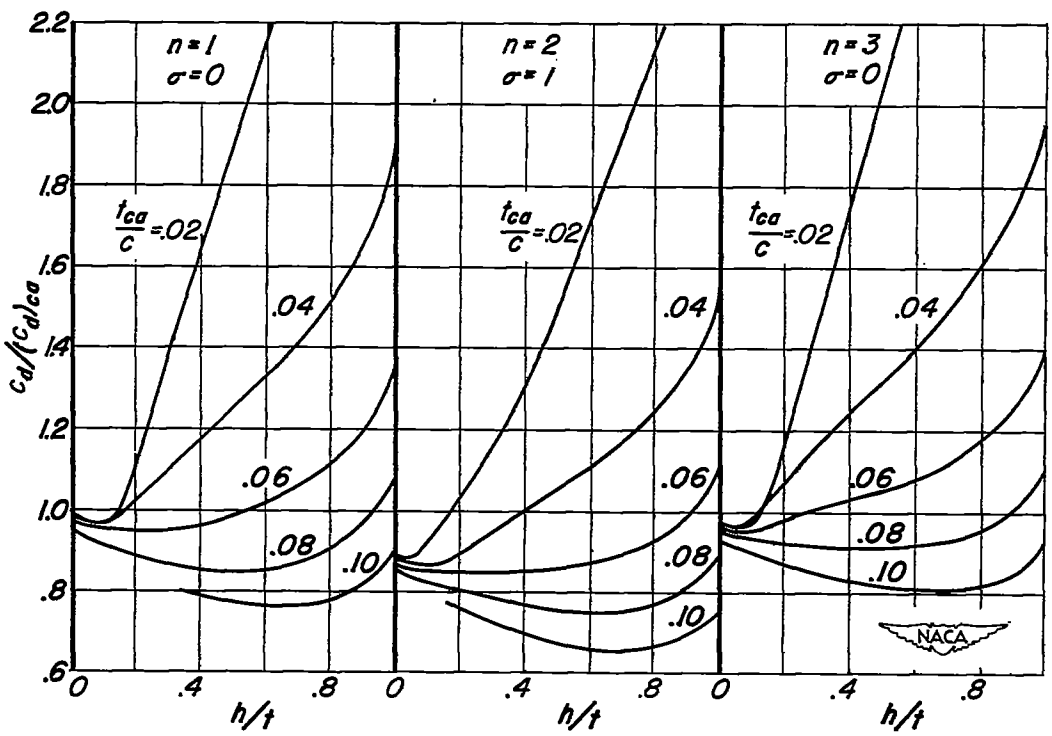

(a) M_∞=1.5, p_b corresponding to turbulent flow at Re=10^7

Figure 12.-Effect of trailing-edge bluntness on the relative pressure drag of semioptimum profiles compared to a structurally equivalent circular-arc biconvex profile.

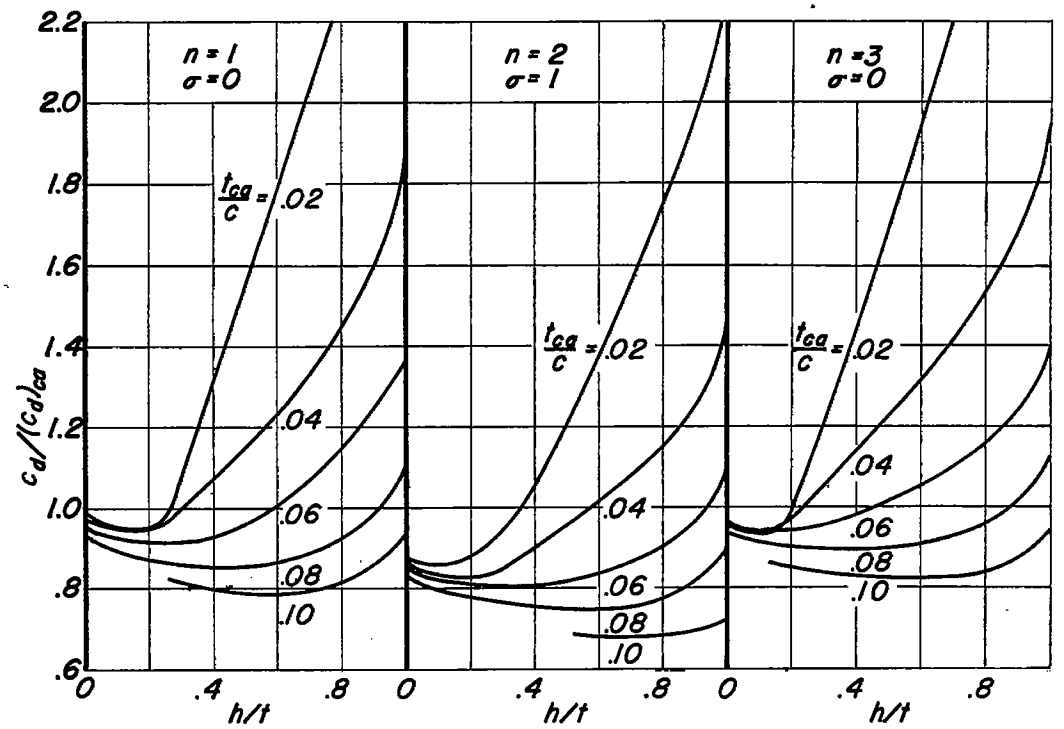

(b) $M_\infty = 3$, p_b corresponding to turbulent flow at $Re = 10^7$.

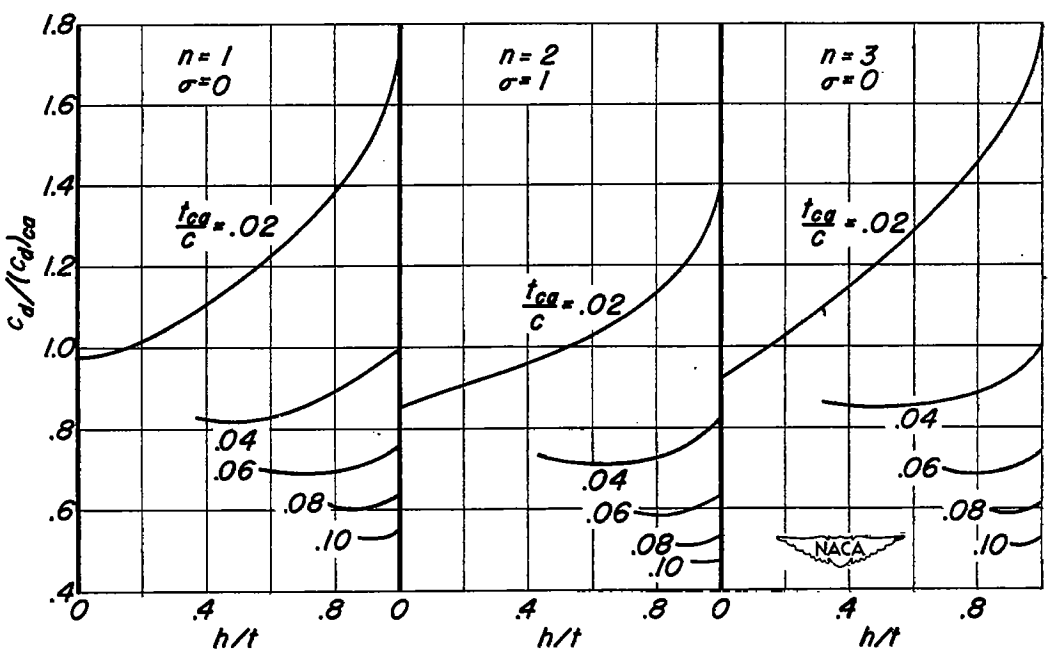

(c) $M_\infty = 8$, $p_b = 0.1 p_\infty$ (assumed).

Figure 12. — Concluded.